FIELD VALIDATION OF INSITU SUBGRADE RESILIENT MODULI VIA FALLING WEIGHT DEFLECTOMETER BACKCALCULATION METHODS

By

JACOB MATTHEW TOWNSEND, EIT

(Under the Supervision of S. Sonny Kim)

ABSTRACT

The subgrade resilient modulus values of Georgia counties are based upon historic soil support values, but with the increasing implementation of the 1993 AASHTO Pavement Design Guidelines and the initial adoption of the MEPDG system, more accurate subgrade resilient modulus values are required. To identify proper values and accelerate their adoptions, falling weight deflectometer paired with ground penetrating radar can quickly determine the back calculated resilient modulus values and validate the insitu subgrade stiffness and be compared to the implemented soil support values, without extensive laboratory testing procedures. Thus, decreasing the testing cost and time for pavement engineers to understand the design values for roadway subgrades.

INDEX WORDS: Falling Weight Deflectometer, Field Validation, Resilient Modulus

FIELD VALIDATION OF INSITU SUBGRADE RESILIENT MODULI VIA FALLING WEIGHT DEFLECTOMETER BACKCALCULATION METHODS

By

JACOB MATTHEW TOWNEND, EIT

B.S. University of Georgia, 2021

A Thesis Submitted to the Graduate Faculty of The University of Georgia in Partial Fulfillment of the Requirements for the Degree

MASTER OF SCIENCE

ATHENS, GEORGIA

2022

FIELD VALIDATION OF INSITU SUBGRADE RESILIENT MODULI VIA FALLING WEIGHT DEFLECTOMETER BACKCALCULATION METHODS

By

JACOB MATTHEW TOWNSEND, EIT

Major Professor: S. Sonny Kim

Committee: Jidong Yang
Stephan Durham

Electronic Version Approved:

Ron Walcott
Vice Provost for Graduate Education and Dean of the Graduate School
The University of Georgia
May 2022

DEDICATION

Thank you, Nana, for keeping family close. I love and miss you every day.

Sue Townsend Dyer

November 12, 1950 – October 10, 2021

ACKNOWLEDGEMENTS

Thank you, Dr. Kim, for your support over the past few years and allowing me to be a part of your research team as I develop the foundations of my career and life as an engineer for all. Thank you to the other members of my committee Dr. Durham and Dr, Yang, I have appreciated your direction and engineering knowledge you have passed down to me. Thank you to the University of Georgia College of Engineering for letting me develop as an engineer while wearing Red and Black. Thank you to all my fellow classmates and fellow engineering students, you make UGA and Athens a special place to be. Thank you, Abigail, for your support and keeping me motivated on many late nights of work. Lastly, thank you to my family for your continued support as I chase my dream, I will make you all proud.

TABLE OF CONTENT

LIST OF FIGURES

LIST OF TABLES

This page was left intentionally blank

CHAPTER 1 INTRODUCTION

1.1 Background

Current pavement design methodology for many state and federal Department of Transportation agencies is conducted under the 1972 and 1993 *AASHTO Interim Guide for Design of Pavement Structures*. While the most recent guide has been in use for nearly 30 years, the empirical data used to develop the guide were derived from procedures conducted during the 1960's AASHTO Road Test. To overcome the limitations of empirical design, Project 1-37A of the National Cooperative Highway Research Program proposed a mechanistic-empirical pavement design guide (MEPDG) in the *Guide for Mechanistic-Empirical Design of New and Rehabilitated Pavement Structures* (ARA, Inc., 2004) to replace the empirical procedure in the AASHTO design guide. The MEPDG aims to provide a more complete pavement design methodology by implementing mechanistic-empirical based inputs for pavement layers, material properties, traffic loadings, climate conditions, and more. These inputs are structured on a basis of hierarchical levels (1, 2, and 3) that provide the engineer with flexibility over the accuracy of their design. Among these inputs is resilient modulus for subgrade layers which is a composite mechanical property of subgrade materials and characterizations of subgrade stiffness behavior. Some agencies consider the cost, time, complication, and sampling resolution required for meaningful resilient modulus testing to be too cumbersome for its application in less critical projects. Regardless of project size, it is often difficult to predict and consequently reproduce the in-situ conditions, usually with respect to the state of stress and moisture condition, further complicating the use of resilient modulus testing.

Resilient modulus is defined as the ratio of the amplitude of the repeated axial stress to the amplitude of the resultant recoverable axial strain. As a result, it is a highly regarded performance metric for pavement design applications and remains a premier input in all three design input levels of the MEPDG. Specifically, the resilient modulus is relied upon to determine overall subgrade stiffness and ability to support the above road surface layers with minimal cracking.

Conducted under AASHTO T-307 testing procedure, resilient modulus determination may be a difficult and expensive procedure to perform in the laboratory. Overtime back-calculation methods from Falling Weight Deflectometer (FWD) field data for resilient modulus have led to the current generation of a variety of accurate prediction models. These models often prove sufficient for global applications, but the wide array of in-situ subgrade properties limits their precision when evaluating project-specific samples. Therefore, among the objectives of this study is the collection of field data for the initiation of a machine learning model for resilient modulus prediction using other existing subgrade exploration methods such as FWD and Ground Penetrating Radar (GPR) techniques. These efforts intend to provide supplemental value to the existing materials library utilized in pavement design practices in Georgia.

Implementation of the MEPDG for state Department of Transportation (DOT) agencies is a lengthy, multi-step process that requires local calibration, operational processes integration, traffic and climate data collection, material database development, and more. The Georgia Department of Transportation (GDOT) is among the state highway agencies conducting such efforts to improve their current practices, conducted under the 1993 AASHTO Interim Guide for Design of Pavement Structures. These efforts were supported by several cooperating agencies such as Applied Research Associates (ARA) and local universities including the University of Georgia (UGA).

The Geotechnical and Materials Engineering Laboratory (GMAT Lab) at the University of Georgia has been at the forefront of resilient pavement design and monitoring in recent years. The GMAT lab has partnered with GDOT on several research projects involving different aspects of geotechnical and pavement engineering design. Recently, the GMAT Lab has been involved with several research investigations into resilient modulus laboratory testing, insitu proximal and remote mapping, as well as development of machine-learning based prediction algorithms. Several of the projects that the GMAT lab have partnered with GDOT will be summarized below. The GDOT Research Project 12-07, “Measurement of Dynamic and Resilient Moduli of Roadway Test sites”, (Kim, 2013) investigated laboratory testing of resilient modulus according to AASHTO 307-99 procedures. The report covered subgrade samples collected from 9 different borrow pits from across Georgia. The project data developed an initial database of resilient modulus values from across the state for GDOT use in pavement design work. The project laid the groundwork for GMAT’s involvement with subgrade research and catalyzed several years of positive cooperation with GDOT research teams. The next iteration of resilient modulus research was in cooperation of the GDOT research Project 17-25, “Prediction of Resilient Modulus from Laboratory Testing of Sandy Soils”, Kim and Phano et. Al. 2019, in which datasets from other GDOT subgrade investigations were correlated with resilient modulus data from the laboratory testing. The project investigated the utilization of soil index test, porosity and permeability, and proctor density testing to identify possible correlations. An artificial neural network (ANN) was also implemented to develop a prediction model for resilient modulus based off the various inputs. The report yielded a model based off the optimal moisture content (OMC) density value for subgrade. These projects help initialize and expand GDOT’s MEPDG inputs based off laboratory and field-testing values to assist in the state agencies transition from the AASHTO 1993 Pavement Design Guide to the

MEPDG standards. However, both projects required extensive laboratory testing or other destructive field-testing procedures to achieve the resilient modulus data. So, this report aims to collect proximal roadway subgrade data via FWD and GPR and develop mathematical correlations between the datasets.

1.2 Problem Statement

With an ever-increasing road network in the United States, the need for better road conditions and performance evaluation methods are necessary. The process of road scanning for maintenance and layers testing is considered an expensive process, resources consuming, and time-consuming. Traditional methods lack the quantifiable methods that are currently achievable from modern technologies and practices. Further need to investigate and understand subgrade performance over time and throughout conditions can assist pavement engineers with rapid, current quantifiable pavement performance and condition.

1.3 Project Objectives

1. To verify existing GDOT resilient modulus database from historic methods with FWD back calculated methods
2. To verify roadway section stratification from extracted cores with ground penetrating radar scans of targeted areas
3. Initialize the development machine learning techniques to predict subgrade resilient modulus from GPR data

1.4 Significance of Research

1. The primary benefit of this study is to guide pavement engineers to conduct a successful road evaluation practice for the current service roads. Knowing the relationship between

subgrade soil properties and surface condition summarizes most of the terms to decide on road serviceability.

2. This study focuses on the application of proximal sensing and machine learning in modeling soil attributes.
3. By utilizing continuous scanning methods more accurate resilient modulus parameters can be used for roadway agencies.

CHAPTER 2 LITERATURE REVIEW

2.1 Overview

The following chapter will review previous work conducted on the subsystems utilized in the research of the topic. Emphasis will be placed on historic development of resilient modules calculations, theoretical background for pavement investigation, and implementation of different technologies to increase the prediction of pavement performance metrices.

2.2 Resilient Modulus

Pavement designs have always centered around the fundamental concept of transporting heavy goods across long surface distances as quickly and efficiently as possible. All pavement designs complete the primary objective of ground-based transportation by stratification of compacted materials such as asphalt and concrete on top of other support materials like gravel and crushed rock which all lay atop of the natural subgrade of the environment. Since all pavements rest upon the insitu subgrade, the derived strength of a pavement section is based upon the capacity of the subgrade layer, so an intimate understanding of soil mechanics and behavior characteristics is crucial. To be able to resist the moving loads of vehicle traffic, subgrade materials need to be in a compacted state to resist significant deformation. Besides soil mechanics, pavement structures also rely on critical factors such as, climate conditions and traffic type, volume, and frequency.

The forefront of roadway research and policy has been the American Association of State and Highway Transportation Officials (AASHTO) which had its inception in 1914 and early policy and legislation push in 1916 as part of the United States federal highway construction act. In the late 1950's, a series of pavement test were conducted, named the AASHTO Road Test, which was the largest road experiment, totaling around $27 million, at the time. The information obtained from the AASHO Road Test was crucial in advancing knowledge of pavement structural design, pavement performance, load equivalencies, climate effects, and much more. The basic performance information resulted in the performance equations and nomographs used in the AASHTO design guides beginning in 1961 and revised again in 1972. In the early AASHTO guides, the subgrade was characterized in Soil Support Value (SSV) which a scale from 0 to 10, and a value of 3 was used to represent the natural subgrade found in Illinois, USA, which was the insitu subgrade in the AASHTO Road Test.

The 1986 AASHTO design guide for flexible pavement design replaced the historic soil support value and recommended the use of resilient modulus Mr for the primary subgrade characteristic that can be used for mechanistic analysis of pavement systems. Since the 1986 adoption, Mr has been widely utilized for pavement design and evaluation. Resilient modulus is the ratio of the applied deviatoric stress versus recoverable strain and is conservatively estimated as the elastic modulus for soil. Resilient modulus also considers viscoelastic properties such as stress state and temperature of the subgrade material.

Resilient Modulus: $Mr = \sigma_d/\varepsilon_r$ (2.1)

Where:

σ_d = Applied deviator stress

ε_r = Resilient strain

In 1993 AASHTO vastly updated its pavement design curriculum with the culmination of pavement research and analysis methods and yielded in the 1993 AASHTO Guide for Pavement Structures. The 1993 design guide listed 4 different methodologies for determining resilient modulus for pavement designs. The different methods consisted of laboratory testing, correlating

Mr from other subgrade physical properties, back calculating moduli from Non-Destructive Testing (NDT) methods, and lastly moduli values from insitu construction data. Over the years, the 1993 AASHTO design guide became the primary analysis methods used by Federal and state Highway agencies, and each have used several iterations of the resilient modulus calculation methods previously mentioned.

The subgrade resilient modulus laboratory testing procedures are laid out according to AASHTO T307-99 (2021) “Standard Method of Test for Determining the Resilient Modulus of Soils and Aggregate Materials”. The AASHTO testing summary states, “A repeated axial cyclic stress of fixed magnitude, load duration (0.1 s), and cycle duration (1.0 to 3.1 s) is applied to a cylindrical test specimen. During testing, the specimen is subjected to a dynamic cyclic stress and a static-confining stress provided by means of a triaxial pressure chamber. The total resilient (recoverable) axial deformation response of the specimen is measured and used to calculate the resilient modulus”.

Figure 1: Typical Triaxial Loading Device and Chamber

The purpose of the distinctive, repeated load pulses that are utilized in the test is to mimic the loading pattern of a heavy vehicle wheel quickly loading and unloading a specific point. Also, the confining pressure of the triaxial chamber can recreate the confining pressure experienced by insitu subgrade from overburden pressure compounded by the axial pressure from the vehicle wheel path. To understand the viscoelastic properties of soil with resilient modulus, 3 confining pressures with 5 different deviatoric stresses are applied to the repeated load triaxial chamber. With the 15 resilient modulus values, a model is derived to best-fit the data of each sample so the resilient modulus of a desired stress can be obtained as demonstrated through Figure 2, by AASHTO (2021).

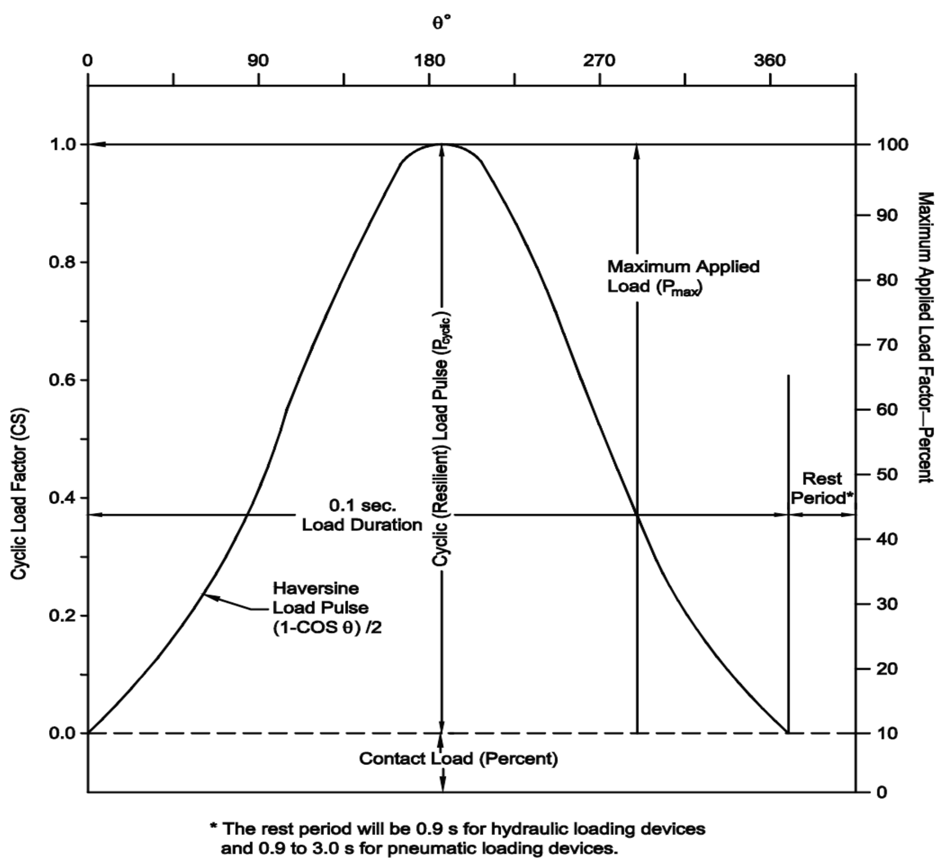

Figure 2: Typical Resilient Modulus Cyclic Axial Load Curve

The resilient behavior of unbounded subgrade materials from nonlinear stress states have been thoroughly explored and Kim et. al. (2004) demonstrated that the performance output emphasis a significant degree of importance on the effect of deviatoric stress, dry density, moisture content, gradation and shape, fines content, and stress state. The report yielded that an increase in dry density or degree of compaction of granular materials makes the aggregate matrix stronger and stiffer. Previous research indicated that the effect of dry density or degree of compaction has been considered as the significant influencing factors for the resilient behavior of unbound granular materials, by increasing the Mr with increasing dry density Kim et. al. (2004). Kim et al. (2007) also mentioned that the effect of the dry density decreases with increase of fine content and varies with the aggregate types and stress states.

A change in aggregate gradation produces a change in moisture content and dry density to form an appropriate aggregate assembly and the moisture content of unbound granular materials significantly affects the resilient response (Kim et al, 2007). The initial increase of stiffness is due to the increase of the contacts as voids are filled with fines and the decrease of stiffness is due to the displacement among coarse particles as excess fines are added. This results in the loss of aggregate particle interlocks and load carrying ability lies only on the fines. To investigate the effect of gradation on subgrade resilient modulus, Kim et al. (2007) proposed the use of a three-parameter equation to quantify the full-scale particle size distributions. This three-parameter equation used to fit cumulative distribution functions of aggregate gradations is shown in the equation listed below:

$$P_p = \frac{100}{\ln\left[\exp(1) + \left(\frac{g_a}{d}\right)^{g_n}\right]^{g_m}} \tag{3.2}$$

Where:

Pp= the percent passing a particular grain size diameter, d, measured in mm,

ga = fitting parameter corresponding to the initial break in the grain-size curve,

gn = fitting parameter corresponding to the maximum slope of the grain-size curve,

gm is a fitting parameter corresponding to the curvature of the grain-size curve.

Non-linear regression analyses were performed to obtain a set of parameters that fit a specific gradation. When the gn and gm are fixed, the parameter ga is related to the percent of coarse aggregates. The parameter gn controls the slope of the gradation curve, which determines if the gradation curve is open, gap or well graded. When the value of the parameter gn increases, the gradation moves toward a gap-gradation, and differences between the slopes in the early and latter portion of the curves become more severe.

It has been also known that the stress state is an important factor influencing resilient properties of unbound granular materials. They have shown that the MR of unbound granular materials depends on the confining stress and sum of principal stresses. It is generally agreed that the MR increases with increasing confining stress and decreasing deviatoric stress

The T307-99 AASHTO Mr Triaxial test, AASHTO T-89 (Liquid Limit Test), and AASHTO T-90 (Plastic Limit Test) were utilized to develop a level 3 input database for MEPDG Mr inputs by testing subgrade samples from 9 different subgrade sources from across the state of Georgia. Kim et. al. (2013) noted a reduction in tested stress states from 15 to 12 would be useful for the level 3 MEPDG input and increase the speed of testing required. An Artificial Neural Network (ANN) was developed to predict the Mr from the other laboratory testing procedures with a notable degree of success R^2=0.86 but notes that the developed ANN can reasonably predict Mr based off stress state inputs locally in Georgia.

In a later study, Kim et. al. (2019) determined the results from laboratory resilient modulus testing can vary because of location of the measurement system, testing stress sequences, and compaction methods, which vary among the test methods available for use. Therefore, correlations developed by other researchers may not produce similar results. The correlation model developed can be used to predict resilient modulus for coarse-grained soils, was based upon optimal moisture content (%OMC) of the subgrade. It is stipulated that it should be compared to available test data before a resilient modulus is selected for pavement design with the MEPDG.

$$M_R\ (psi) = 23{,}850.435 - 825.7241(\%OMC) \qquad (3.3)$$

The model for predicting subgrade resilient modulus in (Kim, 2019) was based upon correlation from other soil testing datasets and physical properties of the subgrade. The testing procedures utilized in (Kim, 2019) were the Lifting Weight Deflectometer (LWD), Dynamic Cone Penetrometer (DCP), and Ground Penetrating Radar (GPR) systems, whereas the soil index properties dataset was collected by GDOT as used for other pavement design procedures. The same 9 locations as (Kim, 2013) were utilized to compare the results of the two reports. The report concluded that the subgrade resilient modulus predictive model presented should be used to select design values for subgrades constructed of coarse-grained materials. The predictive values should then be compared to available laboratory and/or field test results until a level of comfort with its use can be attained. The report also concluded that other a insitu predictive method should be developed to more accurately predict the subgrade resilient modulus at a site, for use in MEPDG design inputs.

As previously highlighted, the laboratory testing procedures are a time consuming and costly process for various pavement design agencies due to the amount of testing required for a road network system with a variety of insitu subgrade types. Besides laboratory test, other prescribed measures for determining resilient modulus are correlating resilient modulus values to other soil parameters that are more accessible to pavement engineers. Such examples of correlating resilient modulus are California Bearing Ratio (CBR), R-value, and soil index testing. CBR soil testing was initially developed by the California Division of Highways in the 1930's and has seen a widespread adoption as a subgrade load capacity laboratory testing procedure. Many pavement agencies have developed subgrade resilient modulus comparisons where the CBR ratio from lab testing was multiplied by a single coefficient to obtain a resilient modulus value. The first subgrade resilient modulus correlation to CBR was established by Heukelom W. and Foster (1960) resulting in Equation 2-4.

$$Mr(psi.) = 1565\ x\ CBR \tag{2-4}$$

Later, the Heukelom and Klomp correlation, Equation 2-5, was established and is still used by many state agencies today.

$$Mr(psi.) = 1500\ x\ CBR \tag{2-5}$$

The CBR estimate has seen slight changes to the coefficient over the years in a report by Dione et. al. (2015), a resilient modulus prediction model was developed for MEPDG implementation, where resilient modulus laboratory testing was compared to Equation 2-4 and Equation 2-5 Mr and CBR correlations. The report concluded that the Mr-CBR relationships tend to overpredict or underpredict the resilient modulus of the unbounded subgrade depending on soil type. The 1993 *AASHTO Interim Guide for Design of Pavement Structures* incorporates the Heukelom and Klomp equation but includes soil data that ranged from 750-3000 times the CBR value. The soil test data included various types of soil and coefficients to be as widely usable as possible. However, the equation requires certain parameters such as soaked soil CBR values less than 10 for fine-grained soils. Specifically, the study shows that the CBR equation can over predict subgrade resilient modulus when CBR > 5 and under predict, high CBR value soils.

A subgrade resilient modulus prediction based upon laboratory testing procedures, ASTM D2844 -18, *Standard Test Method for Resistance factor R-Value and Expansion Pressure of Compacted Soils* or R-value Test. The R-Value Test measures the potential strength of subgrade, base, and base course materials in roadway sections. The Asphalt Institute (developed correlations between resilient modulus and the constituents R-Value, Equation 2-6 for subbase and course base roadway materials, and Equation 2-7 for fine grained soils.

$$Mr(psi.) = A + B\ x\ (R - Value) \tag{2-6}$$

Where:

A = 772 to 1155

B = 369 to 555

$$Mr(psi.) = 1000 + 555\ x\ (R - Value) \tag{2-7}$$

The results of Equation 2-7 is to be used as an initial design value criteria until localities develop region specific values based upon are data collection programs per agency. However, R-Value Test require extensive, intrusive soil testing procedures to be utilized with high degree of accuracy in the field.

Since the limited success of resilient modulus correlations with CBR testing due to variability of the subgrade resilient modulus prediction, other testing methodologies have been investigated to further improve the accuracy of correlation methods. Hossain et. al. (2014) demonstrated the Mr-CBR correlation can vary significantly based upon soil type and proposed utilizing unconfined compressive strength test with other soil parameters are more accurate and apply to a greater variety of soil types.

Moisture content and compaction have been identified as important aspects in predicting subgrade resilient modulus. Hossain et. al. (2009) reported that the modulus of frozen soils can rise 20 to 120 times the modulus before freezing occurs. Also, an inverse relation was identified with resilient modulus and the degree of saturation of the soil. Other researchers have found similar moisture effects throughout the year, where modulus can increase during the dry season and decrease during the wet season, higher and lower moistures swings from the optimum moisture content will decrease the resilient modulus. Therefore, proper modeling of the moisture conditions is necessary to select the correct modulus because a modulus too high can result in thinner section than is required. A modulus too low will result in too thick a pavement section and the unnecessary expense in materials.

Researchers have utilized several of the identified key factors for Mr prediction leading due a wide array of different statistical analysis methods to further develop more specific prediction equations. Long Term Pavement Performance (LTPP) studies conducted by Malla and Joshi et. al. (2008) has reviewed various federal agencies LTPP data where a model was developed to estimate the Mr of base layer and non-cohesive AASHTO A-2-4 subgrade soils that are commonly available in the state of New Mexico from a set of materials physical properties. They concluded that soil type played a significant role on Mr prediction with some subgrade types not accurately represented by several of the investigated models. Work undergone by George et. al (2004) shows that higher cohesion soils like AASHTO A-5, A-6, and A-7 do not follow the standard LTPP equations and simpler equations should be employed cautiously. Other state specific studies such as Kim et. al (2013) where laboratory Mr data from 9 different road subgrade borrow pits were analyzed and linear regression models developed. In the 2013 report, a Mr prediction model was developed based upon a linear regression of subgrade water content, plasticity index, and confining pressure utilized in the laboratory triaxial test.

2.3 Nondestructive Testing Methods

Outside of the previously mentioned methods to determine resilient modulus, the 1993 AASHTO design guide also lays out technique's agencies can use to determine Resilient Modulus from back calculating methods derived from various non-destructive testing (NDT) methods. Although the prescribed methods were considered rudimentary and only for experimental research, since then, significant focus has been directed towards NDT methods for roadway and subgrade condition and performance. Several different studies have focused on determining alternative NDT methods for correlating Mr from the soil stiffness parameters derived from Light Weight Deflectometer (LWD), Falling Weight Deflectometer (FWD), and Ground Penetrating Radar (GPR) technologies. At this time, LWD testing on subgrade and roadways has been limited to handheld testing because the resulting elastic modulus only consider a single stress state point compared to resilient modulus. Lastly, LWD testing has seen smaller emphasis compared to FWD testing because the consistency of results, and ability to automate the testing procedure. These factors are why FWD testing is more widely adopted by various roadway agencies for NDT field testing procedures.

2.3.2 LWD Testing

LWD laboratory testing has been investigated as a method of determining subgrade resilient modulus by combining different drop heights, weights, and deflector plate sizes. In a report by

Tihey and Kim et. al. (2020) explores how different LWD parameters effect the accuracy of predicting soil modulus (E_{LWD}). The investigated soil type was a USCS inorganic silty clay (MH) with 6 different moisture content and compaction levels resulting in 6 different densities. Each experiment group test data included 2 different plate sizes 150mm and 300mm, and 4 different drop heights of 6,8,12, and 24 inches. The average soil modulus was determined from each and plotted against varying input parameters such as deflectometer plate size, moisture content, density, and dielectric constant from GPR testing was included. A power model to predict soil modulus from these parameters was derived and lead to R^2 value of 0.858. However, due to the low number of distinct data points used to derive the model, the results are to be implemented cautiously and may overpredict the actual soil modulus (E_{LWD}).

Figure 3: Typical Dynatest® LWD Testing Device

Pavement deflection testing is a quick and easy method for assessing a pavement section's condition compared to more in-depth laboratory testing procedures. With the development of complex, modern deflection measuring devices roadways can be analyzed for various design and construction criteria such as seasonal variance, overlay requirements, and subgrade support conditions. Today, pavement deflection testing is an essential part of road network evaluation and rating, and several roadway agencies have whole departments tasked with roadway testing procedures, such as the GDOT Office of Materials and Testing (OMAT).

2.3.3 FWD Testing

Currently, impulse load testing such as, Falling Weight Deflectometer testing has been the most utilized field NDT method for roadway and subgrade evaluation and has worldwide adoption due to its deplorability at scale compared to LWD laboratory methods. As sown in Figure 4 below, the FWD is like LWD where a known weight is released on to a bearing surface and load plate where a force like a vehicle wheel load is transferred to the underlying pavement surface. A series of sensors are located at fixed distances so the deflection can be measured.

Figure 4: Typical Dynatest® FWD Testing Device

The mathematical basis of deflection-based testing is basic engineering mechanics of solid materials. As Figure 5 from the 1993 AASHTO design guide below demonstrates (FHWA 2017, pg. 31), to back calculate the subgrade resilient modulus, the road section is simplified as a simply supported beam, and the drop weight is symbolized as a single point load dropped along the midpoint of the beam. The maximum deflection at beam center and deflection from center equations are based upon this simplified analysis. Field data concurs this simplified approach by the spaced geophones detecting the deflection of the section from each drop. However, the deflection pattern from center is also dependent upon pavement type with PCC sections having a more linear pattern than the parabolic deflection basin of a HMA section.

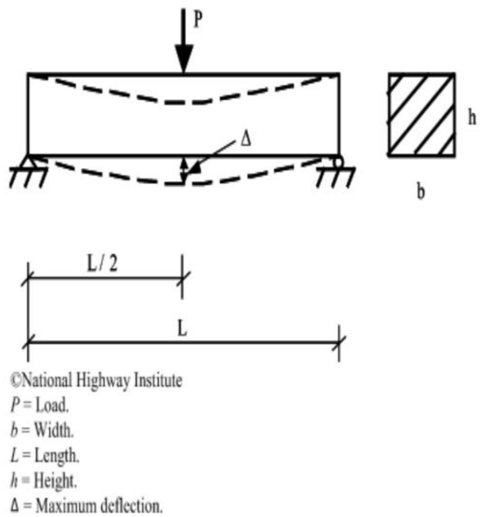

$$\boxed{\Delta = \frac{PL^3}{48EI}}$$

Figure 30. Equation. Maximum deflection of a beam under a fixed load.

Where:

Δ = Midspan deflection of the beam.
P = Load applied to the surface.
L = Beam span.
E = Elastic modulus of the beam.
I = Moment of inertia for a rectangular beam.

The moment of inertia for a rectangular beam I can be determined from the width and height of the beam, as shown in figure 31.

$$\boxed{I = \frac{bh^3}{12}}$$

Figure 31. Equation. Moment of inertia of rectangular beam.

Where:

b = Beam width.
h = Beam height.

Finally, the elastic modulus of the beam (E) can be calculated by substituting the known values of P, L, b, and h.

<u>Figure 5: Derivation of FWD Deflection Model</u>

Compared to other methods FWD utilizes larger testing platforms that can mimic the loading pattern those vehicles produce by imparting a dynamic load to the pavement section. Since FWD replicates the quick dynamic loading conditions of a moving wheel load, more repeatable testing can lead to a greater sample frequency than can be obtained versus more traditional, slower methods. With the structural condition data requirements for MEPDG to develop accurate roadway assessments, FWD has become a fundamental component for data collection procedures of different agencies because of the ability to acquire repeated site-specific condition data. An integral part of the FWD data is the pavement layer elastic modulus and subgrade resilient modulus which are both derived from the magnitude of the loading and resulting deflection data of each layer with known depths. FWD can achieve a higher density of data because it utilizes a system called deflection basin, where a concentric series of sensors are scattered around the central deflection point. which yields deflection data from a larger area versus maximum deflection point methods as illustrated in Figure 6 below (FHWA 2017, pg. 5).

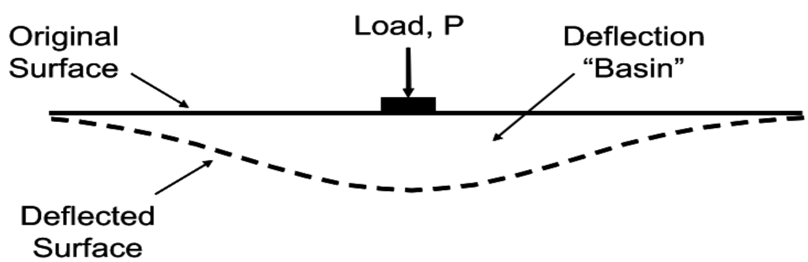

Figure 6: Typical Pavement Deflection Basin

The acquired deflection data has several uses and can characterize pavement conditions based off different parameters. A simple plot can be generated, and the deflection data can be compared and any nonuniformities can lead to further site-specific information. Repeated deflection data can also provide pavement engineers with insight into the roadway response to environmental factors such as curling from a ground-air thermal gradient, asphalt stiffening, and subgrade support across a varying moisture content throughout the year. Also, FWD testing can also yield the effective modulus (E_P) of the overall pavement structure, which provides roadway engineers with insight into the structural capacity of the pavement section. The effective modulus equation is listed in Equation 2-8.

$$d_0 = 1.5\, p\, a \left\{ \frac{1}{M_R \sqrt{1 + \left(\frac{D}{a} \sqrt[3]{\frac{E_p}{M_R}} \right)^2}} + \frac{\left[1 - \frac{1}{\sqrt{1 + \left(\frac{D}{a} \right)^2}} \right]}{E_p} \right\} \tag{2-8}$$

Where:

d_0 = Deflection measured under plate and adjusted to standard temperature, mm (inches)

p = FWD load plate pressure, MPa (lb. /inch^2)

a = FWD load plate area, mm^2 (inch^2)

D = Total thickness of pavement layers above subgrade (inches)

M_r = Subgrade resilient modulus (lb. /inch^2)

E_p = Effective modulus of pavement layers above subgrade (lb. /inch^2)

Despite the area surveyed within the deflection basin, FWD is still considered a quasi-point deflection method and several points need to be gathered across a pavement section. Pavement agencies have established FWD testing pattern and frequency procedures based upon the desired results and condition of the investigated area. For project specific testing, typically 100-to-500-foot spacing intervals are used but can be adapted for location specific requirements such as nearby bodies of water or weak subgrades. Some agencies have also developed network level FWD testing where over 500-foot intervals, and typically only cover a single lane, which are used to gather general indicators for a road network and give insight to targeted FWD testing at a future date.

The FHWA have released several reports that summarize deflection testing methods including some continuous deflection profiling equipment systems such as the experimental

Rolling Wheel Deflectometer (RDD) and the corresponding empirical relations to allow pavement engineers to correlate between the different measuring systems.

2.3.3.1 Factors Affecting FWD Testing

In FWD testing, several factors can affect the output of the deflection data which leads to uncertainty in the raw output data. The factors that affect deflection output have been grouped into 3 different categories according to FHWA reports: structural (Pavement type and thickness), loading (magnitude and frequency), and climate (temperature and seasonal fluctuations). Structural factors are the primary influencers of deflection testing because the testing method itself is a representation of the overall pavement system response to the load. Generally, a weaker system characterized with less supporting subgrade and thinner asphalt layers will deflect more than a thicker asphalt on a stiffer subgrade. However, road material is also an important factor because an asphalt road will deflect more than a concrete roadway of the same thickness, as demonstrate on the figure below (FHWA 2017, pg. 19).

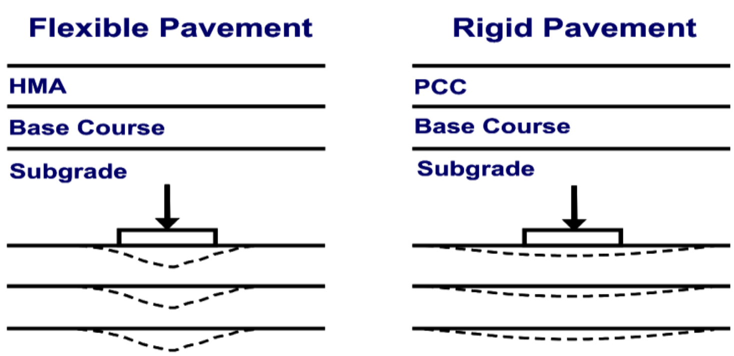

Figure 7: Comparison of Typical Deflection Patterns

Other structural factors include testing location on the roadway such as: edge or joint versus midsection, layer thickness variations, high structural distress, and subgrade variations.

The next group of factors is the loading parameters. Deflection testing is loading dependent, so a slower loading rate will lead to higher deflections, versus a rapid impulse that will yield a smaller deflection. The loading magnitude is also consequential because modern FWD devices are capable of loads ranging from 3000 lb. up to 45,000 lb. for airfield pavements. Determining proper loads is important for pavement engineers to match the conditions experienced on the designed roadway. The most widely used load magnitude is 9,000 lb. because it is representative of a single wheel load for a standard 18,000 lb. axle load prescribed in the AASHTO design guide. The FHWA have developed methods for testing material related distressed in individual pavement sections. One of the developed tests involving FWD is determining the impulse stiffness module (ISM) for a given pavement section. ISM is the ratio of FWD point load versus deflection under the load plate at the (d_0) sensor, Equation 2-9. In PCC pavement sections the ISM_{ratio} is the ratio of the ISM at slab center versus ISM at the slab edge/joint and is used in determining the condition of each slab, Equation 2-10. According to the 2017 FHWA Report, "*Using Falling Weight Deflectometer Data with Mechanistic-Empirical Design and Analysis, Vol1",* An ISM_{ratio} less than 1.50 denotes good condition and ISM_{ratio} greater than 3 denotes a weak joint and needs repair.

$$ISM = \frac{P}{d_0} \tag{2-9}$$

$$ISM_{ratio} = \frac{ISM_{slab\_center}}{ISM_{slab\_joint}} \quad or \quad ISM_{ratio} = \frac{ISM_{slab\_center}}{ISM_{slab\_corner}} \tag{2-10}$$

The final group of variables for pavement deflection criteria is climate conditions. Asphalt and subgrade are viscoelastic materials, so the base temperature of the material can affect engineering properties such as stiffness. Moisture conditions can also affect pavement deflection levels because seasonal fluctuations of ground and atmospheric water saturation amounts. Generally, deflection testing is done in the springtime because the warmer temperature with more saturated conditions lead to higher deflection levels, so pavements and subgrade conditions are measured against these maximum deflection scenarios, as highlighted by Figure 8 below (AASHTO 1993, pg. 212).

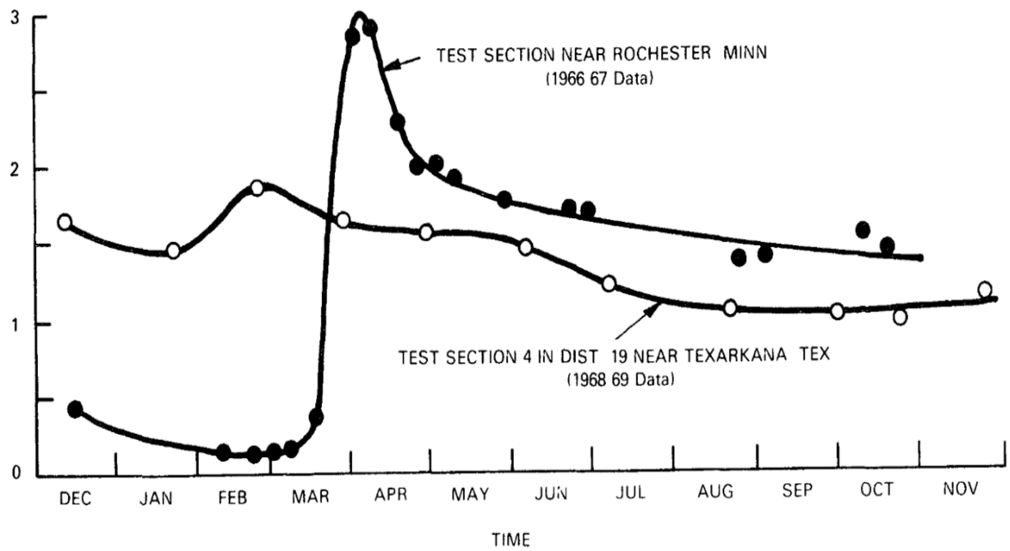

Figure 8: Seasonal Variations of Pavement Deflection

With FWD as a quick and reliable method for non-destructive pavement testing that has lots of controllable variables, it is understandable that this form of deflection testing has seen utilization in agencies around the world. GDOT has amassed a large database of FWD testing for several roadways in many regions of Georgia each with different pavement types, pavement depths, and subgrade materials. However, as previously stated FWD is a point-based deflection testing system so, several import design parameters can be missed due to the innate variability of FWD testing methodologies. Continuous stiffness testing procedures would be ideal when mapping subgrade resilient modulus due to the significant variability possible of insitu subgrade experienced along the length and scope of a road network system.

2.4 Ground Penetrating Radar (GPR)

Soil density has been considered the primary design criteria for soil mechanics and pavement subgrade condition. Traditionally, insitu subgrade density is determined by sand cone test, nuclear gauge devices, and laboratory proctor test. These traditional methods are invasive and require considerable fieldwork to acquire adequate number of samples for testing, which is not feasible for consistent and repeatable field data, so other soil exploratory methods have been researched. With its initial conception and development in the 1930's and famously used in World War II for airplane detection and national defense, electromagnetic radiation (EMR) devices emit radio waves to detect a material change. Initially, ground directed systems were utilized to estimate the thickness of ice sheets and glacial depths. In the 1970s and 1980s, these radar systems saw continued commercial development and the advent of the now called, ground penetrating radar (GPR) was used for pavement structure surveys. The 1980s saw the development of many GPR systems, including vehicle mounted systems, that were initially designed to determine the thickness of a pavement layers. Over time, several other pavement section factors could be determined from the GPR images and empirical models were developed from these early advancements. The significance of GPR utilization for pavement investigation is the speed at which continuous non-destructive pavement surveying can be conducted. Also, GPR produced high resolution geophysical data compared to seismic, radioactive, or magnetic surveying methods, which allow for greater model detail and accuracy. Several engineering applications of GPR have been developed ranging from detecting buried objects such as utility lines and tunneling to infrastructure surveys of large civil structures and bridges as well.

2.4.1 GPR Background

GPR systems are based upon electromagnetic theory (EM) and the change of velocity of electromagnetic waves through a medium. The standard GPR system uses a selected EM wave frequency that propagate throughout the pavement and subgrade system. When a GPR signal is emitted at a point the wave propagates down through the pavement structure and either further penetrates lower levels, scatter through the different mediums, or is reflected to the radar and picked up as the return signal. As Figure 9 demonstrates, the process of wave propagation occurs in a very small amount of time allowing the GPR to pick-up high-resolution data along a thin line parallel to the service vehicles travel path (Abdelmawla 2021, pg. 21).

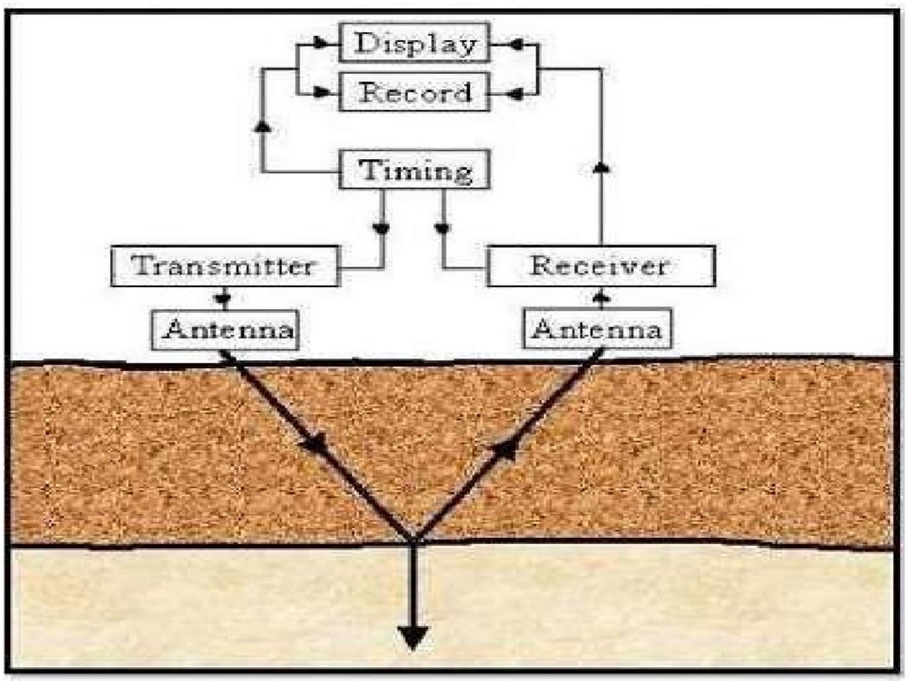

Figure 9: Theoretical GPR Application Flowchart

The main components of an impulse GPR system as shown in figure above, consist of an antenna unit (with transmitter and receiver), a control unit, a data console/display, and a power unit. Impulse GPR systems operate by transmitting a brief EM burst or ‘pulse’ from a transmitter and recording the pulse reflections from features or layers within the pavement as they are returned to a receiver as noted by the arrowed lines.

There are different variants of GPR units with different antenna systems. The two most utilized impulse systems are ground into 2 categories, air-coupled and ground-coupled. Ground coupled radar antennas that require physical contact with the pavement surface. At a given frequency, ground coupled antennas can achieve a greater penetration depth and good for deeper subgrade exploration. The air coupled antennas can sit above the pavement surface allowing for faster data acquisition rates through increased vehicle speed, but do not have the ground penetration depth of ground coupled devices. Also, air coupled devices are typically physically larger devices because the greater frequency required. Air coupled antennas are good for surface and subbase layer exploration, but the data becomes too noisy to use in the subgrade layer.

2.4.2 Dielectric Constant

The primary material property extracted from GPR data is the material dielectric constant. The dielectric constant is also known as relative permittivity (ε_r) of a homogeneous media relative to EM velocity (v) in a material to the speed of light in a vacuum (c). The permittivity of roadways can be very dramatic and varied because the varied mixture of materials with different densities, porosities, and water content saturations. The complex nature of ground directed radar signals with varying signal loss and scattering leads to the development of several models that have been established to derive dielectric values for specific constituents so the GPR return signal can be used to formulate engineering properties instead of a highly noisy signal that cannot be used by pavement engineers. GPR interpretation model considers the dielectric of each material and the volumetric fraction of each as well, so if there is a subgrade section that is primarily made of a single soil type the model will factor the noise created by the smaller fractions and return a factored dielectric constant of the primary constituent and secondary materials. Since soil is composite particle material, the density of soil is dependent upon the individual constituents, so the dielectric constant of a soil is also a function of the dielectric constants of each constituent and their individual volumetric properties as previously stated. The most important physical properties that can affect a subgrades dielectric constant is porosity and water saturation of the soil because water has a much higher dielectric constant value than air which has a relative permittivity value of 1.0 and water is around 80 at 20°C. As a dry soil sample increases in density (decrease in porosity) the relative permittivity increases as well.

As previously stated, the GPR signal travels in a thin line parallel to the units travel direction, so the interpreted data is a 2-dimensional image with depth along the vertical axis and the direction of travel or station along the horizontal. The raw GPR data displays the signal amplitude along a grey scale with a greater intensity yielding a higher amplitude change response from the investigated material, as demonstrated in Figure 10 (Abdelmawla 2021, pg. 28).

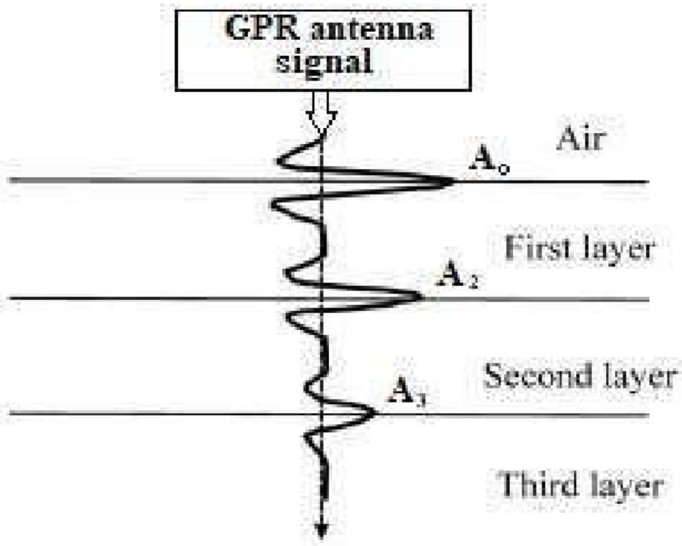

Figure 10: Multilayered System GPR Signal Response Diagram

Once the raw amplitude data is collected the dielectric constant of the different layers can be back calculated from Equation 2-11 and Equation 2-12. The dielectric values of the pavement surface can be calculated from (ε_1) and the subgrade from (ε_{base}).

$$\varepsilon_1 = \left(\frac{1 + \frac{A_0}{A_m}}{1 - \frac{A_0}{A_m}}\right)^2 \qquad (2\text{-}11)$$

$$\varepsilon_{Base} = \varepsilon_{HMA}\left(\frac{1 - \left(\frac{A_0}{A_m}\right)^2 + \left(\frac{A_{base}}{A_m}\right)}{1 + \left(\frac{A_0}{A_m}\right)^2 - \left(\frac{A_{base}}{A_m}\right)}\right)^2 \qquad (2\text{-}12)$$

Where

ε_{HMA}: dielectric constant for the HMA layer

A_0: Amplitude of the surface reflection

A_m: Amplitude of the reflected signal over metal plate on surface for calibration

A_{base}: Amplitude of the reflected signal over the subbase layer surface

2.4.3 GPR Density Model

With the underlying principles of collecting dielectric constant and its theoretical background a density model derived in a GDOT report by Abdelmawla et. al. (2021), was developed to back calculate subgrade density from the dielectric constant data collected from the GPR scans. The power-law approximation Equation 2-13 used is based upon CRIM mixing theory, one of the GPR interpretation models, was the foundation for Abdelmawla density model.

$$\varepsilon_{soil}{}^{\beta} = V_a . \varepsilon_a{}^{\beta} + V_w . \varepsilon_w{}^{\beta} + V_s . \varepsilon_s{}^{\beta} \tag{2-13}$$

This mixing model approximation, combined with empirical relations of various physical soil properties yielded a semi-empirical soil density model dependent upon the soil's relative permittivity and moisture content state.

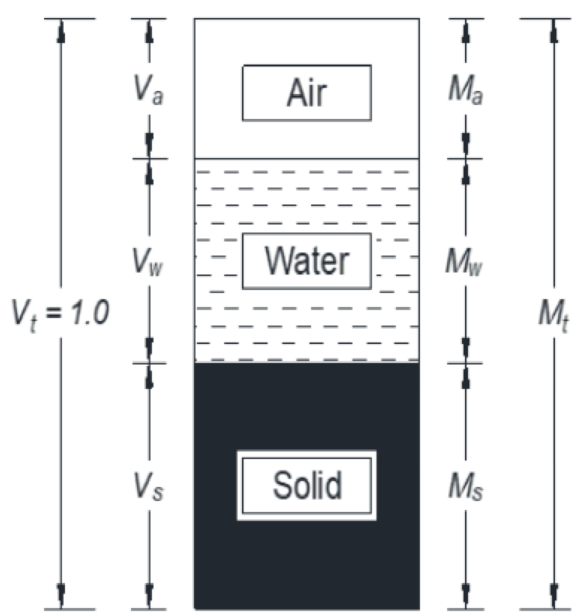

Figure 11: Typical Soil Phase Diagram

Where,

V_a :	air voids volume in soil	M_a :	air voids mass = 0
V_w :	water volume in soil	M_w :	mass of water
V_c :	solid particles volume in soil	M_c :	mass of solids
ε_{coiS} :	soil media dielectric constant	ε_a :	air dielectric constant = 1.0
ε_w :	water dielectric constant = 80–81	ε_c :	soil particles dielectric constant

From phase diagram relations, assuming $V_t = 1.0$,

Based upon correlations of the soil phase diagram and other previously mentioned models, the subgrade dry density model, Equation (2-14) based upon dielectric constant was derived.

$$\gamma_d = \frac{(\sqrt{\varepsilon_{soil}}-1)}{\frac{1}{GS}(\sqrt{\varepsilon_s}-1)+w\,(\sqrt{\varepsilon_w}-1)} \tag{2-14}$$

With the dry density model formulated, a second layer needs to be incorporated to account for the moisture content of the subgrade because of the water content impact on soil relative permittivity. The most used relationship between apparent permittivity, ε, and volumetric soil water content, θ (m^3/m^3), was proposed by Topp et al. (1980), Equation 2-15 is then used to calculate the water content (w), Equation 2-16 of the soil from initial GPR soil density value.

$$\theta = -0.053 + 0.0292\,(\varepsilon_{soil}) - 5.5\times10^{-4}\,(\varepsilon_{soil})^2 + 4.3\times10^{-6}\,(\varepsilon_{soil})^3, \tag{2-15}$$

$$w = \theta \,/\, \gamma_{soil} \tag{2-16}$$

After the water content (w) was calculated, a Generalized Reduced Gradient (GRG) within the GPR model minimizes the error between the estimated and calculated water contents until an acceptable value is reached. This solver process is highlighted in Figure 12 (Abdelmawla 2021, pg. 34).

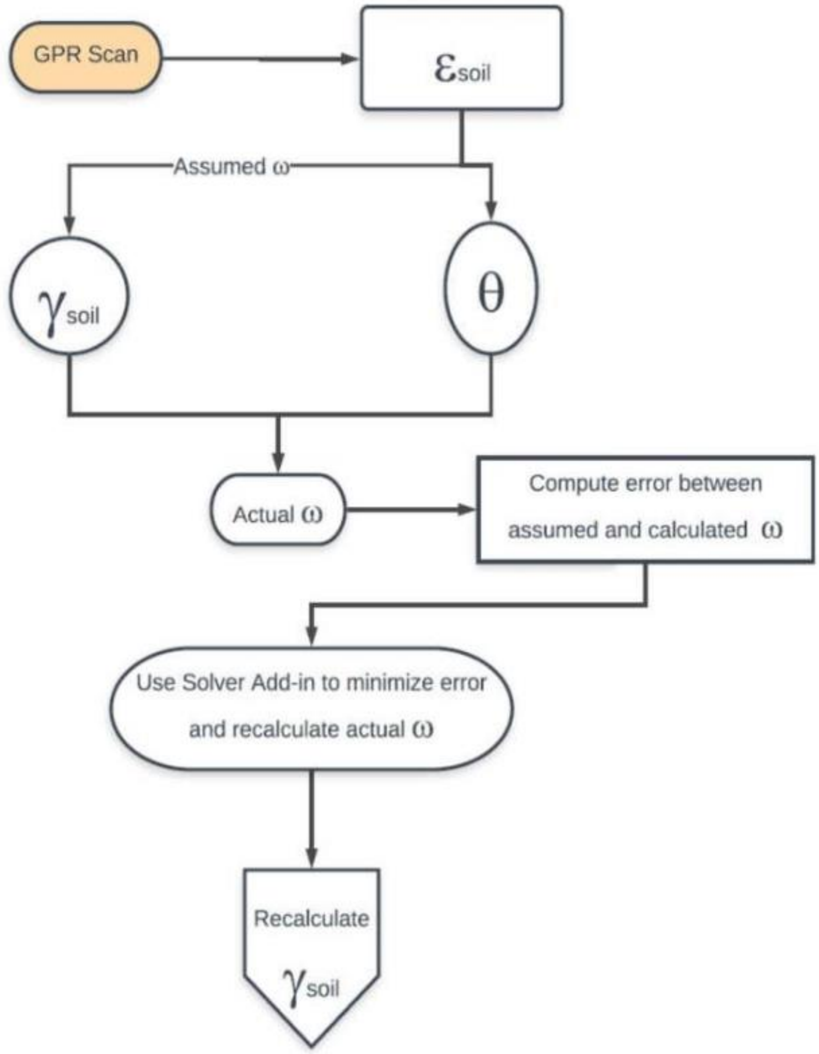

<u>Figure 12: GPR Model Implementation Flowchart</u>

CHAPTER 3 METHODOLOGIES

3.1 Data Collection Overview

The following chapter explores the practices and methods used to collect field data from FWD and GPR proximal sensing systems coupled with roadway cores extracted from selected roadway sites. Figure 13 illustrates how each field examination technique relates to the project objectives in developing a subgrade resilient modulus prediction model.

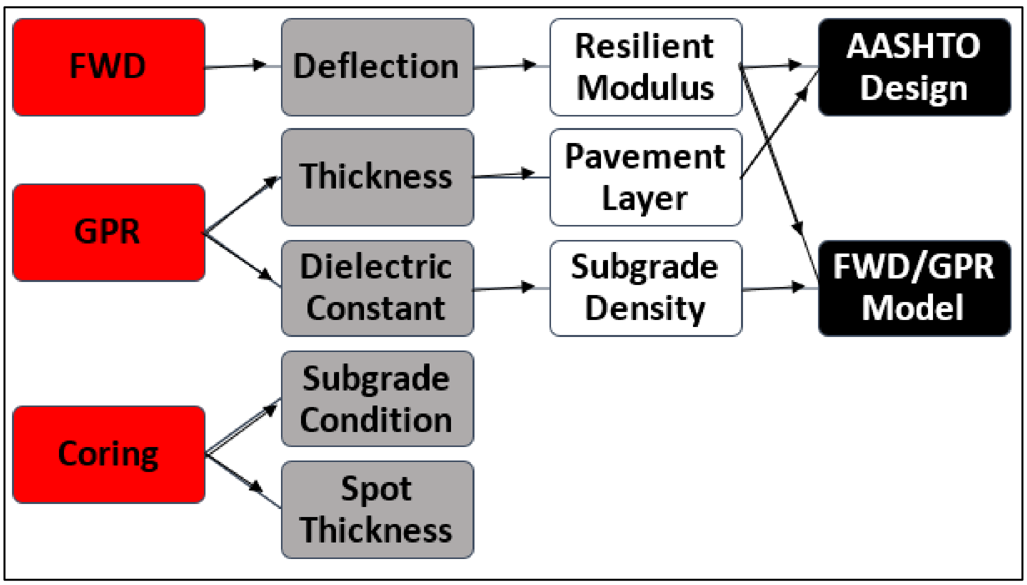

Figure 13: Research Methodologies Overview

The project scope includes 9 different target roadway sections recommended by GDOT across the eastern half of the state. The 9 target roadway sections were selected due to the varied nature of the underlying subgrade, pavement section thickness, and traffic volume across each section. The target roadway sections included in the scope of the project are listed in Table 1, below.

Table 1: Roadway Section Details

State Route (#)	Location (County)	Testing Length (ft.)	Roadway Material	Number of Lanes (#)
10	Walton	9300	Asphalt Pavement	4
11	Walton	5302	Asphalt Pavement	2
22	Hancock	5304	Asphalt Pavement	2
26	Bulloch	5401	Asphalt-over-Concrete	2
57	Emmanuel	5207	Asphalt Pavement	2
57	Johnson	5108	Asphalt Pavement	2
73	Evans	5402	Asphalt Pavement	2
82	Jackson	7702	Asphalt Pavement	2
129	Candler	5328	Asphalt Pavement	2

The target sections are all listed as principal or minor arterial roadways with single unit and multiunit average annual daily truck traffic (AADTT) ranging from 400 to 2,300 units.

field data as well as several extracted cores from each of the roadways also provided by GDOT. The selected routes and total FWD/GPR data set available, and field-testing locations are highlighted in Figure 14.

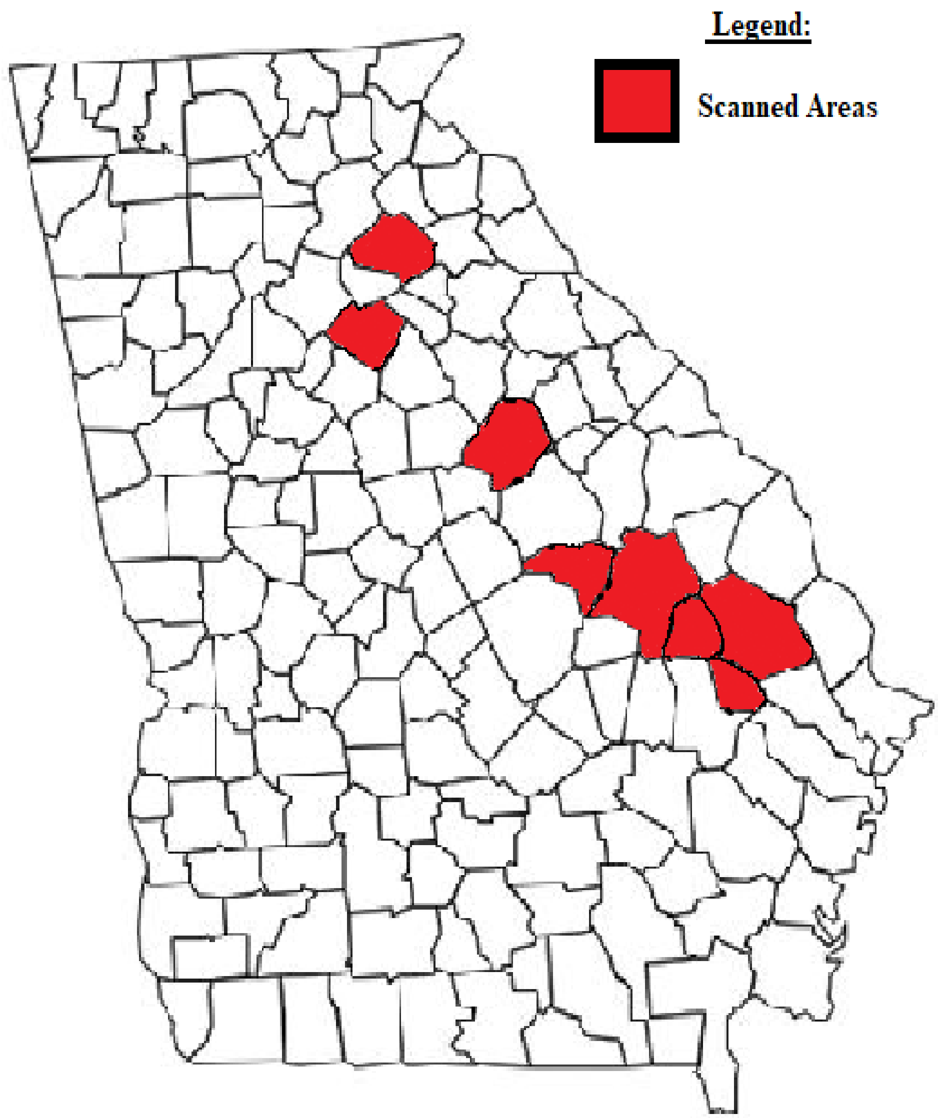

Figure 14: FWD/GPR Testing Locations

The FWD data utilized in this report were collected by GDOT OMAT field teams from May 2021 to July 2021 and packaged as individual file sets. The FWD testing was limited to the slow lane which is congruent with the GPR testing that conducted afterwards along the same lanes and routes and verified by Global Positioning System (GPS) coordinates connected with both FWD and GPR data collection initiatives. At each location, FWD testing was conducted along a preselected 1-mile stretch of the target roadway and had testing deflection basins centered approximately every 100 feet to get a high-resolution deflection database. The FWD field crews conducted 2 sets of 6,9, and 12-kip test loads at each testing location, resulting in 6 drops per station. Standard GDOT FWD procedures utilize the Dynatest 8000 model that captures deflection data via accurate laser measuring devices at set locations away from the impact target area. As shown in Equation 3-1 and Equation 3-2 speed of the laser, speed of light (c), and half of the time to receive the reflected signal back from the pavement can be used calculate the distance in between. The Dynatest FWD system continually captures the calculated distance.

$$v(c) = \frac{distance}{time} \tag{3-1}$$

$$distance = \frac{v(c)}{time/2} \tag{3-2}$$

The lasers target the pavement at 0”, 8”, 12”, 18”, 24”, 36”, 60”, 96”, and 120” from the FWD point load center. The raw FWD testing data provided also includes testing metadata regarding deflections per load, location, time, and the temperature of the air and roadway. The Dynatest FWD testing device utilized is shown in Figure 15.

Figure 15: GDOT Falling Weight Deflectometer Testing Device

3.1.2 Roadway Coring Procedures

While GDOT was conducting the FWD testing, roadway cores were extracted along the target roadway sections to spot check the pavement stratification, thickness, and subgrade or base material composition. The roadway cores were delivered to the UGA GMAT laboratory, see Figure 16, for asphalt property testing, but only the subgrade type and roadway thickness was considered for this report. The roadway cores provided insight into roadway health based upon the volume and size of cracks as seen along the depth of the core, with cores for SR 57 showing extensive cracking throughout. Also, extracted roadway cores for SR 26 revealed varying pavement types since the extracted roadway core composed of layers of both asphalt and PCC materials.

Also, the roadway cores provided information regarding base material composition with the bottom interface of the core either have soil remnants attached, or GAB material sticking to the asphalt layer. GDOT provided roadway section information, see Table 2 and 3, with the extracted roadway cores which confirmed the listed plan base material or provided insight when no supporting base material information was listed, see Figure 16 and 17.

Table 2: SR 11 Core Data Sheet

SR. 11 Walton										
County	**Route**	**Lane**	**Direction**	**Core**	**Station**	**MP**	**AC**	**Base**	**Latitude**	**Longitude**
Walton	11	1	Northbound	1	2003.0	7.19	9.50	Sand-Clay	33.71203904	-83.6994503
Walton	11	1	Northbound	2	3908.0	7.55	10.50	Sand-Clay	33.7168106	-83.6968519
Walton	11	1	Southbound	3	2401.0	7.40	15.00	GAB	33.71486704	-83.6983007
Walton	11	1	Southbound	4	4402.0	7.00	10.00	Sand-Clay	33.70946586	-83.7007969

Table 3: SR 11 Core Data Sheet

SR 22 Hancock										
County	**Route**	**Lane**	**Direction**	**Core**	**Station**	**MP**	**AC**	**Base**	**Latitude**	**Longitude**
Hancock	22	1	Eastbound	1	502	6.605	15.5	Soil-Aggregate	33.22610059	-83.0546048
Hancock	22	1	Eastbound	2	2602	7.005	10.5	Soil-Aggregate	33.23025118	-83.0497816
Hancock	22	1	Eastbound	3	4803	7.425	15.75	Soil-Aggregate	33.23459325	-83.0447279
Hancock	22	1	Westbound	4	504	7.5	15.25		33.23540361	-83.0438718
Hancock	22	1	Westbound	5	2600	7.1	13.25	Soil-Aggregate	33.23126363	-83.0486896
Hancock	22	1	Westbound	6	3501	6.93	12.5	Soil-Aggregate	33.22948141	-83.050763
Hancock	22	1	Westbound	7	4801	6.68	13	Soil-Aggregate	33.22690602	-83.0537477

Figure 16: Extracted Roadway Cores #1

Figure 17: Extracted Roadway Cores #2

3.1.3 GPR Mapping Procedures

GPR testing was conducted by the UGA Geomaterials and Testing (GMAT) lab team with their Vehicle based GPR system. The UGA GPR system includes both a GSSI 2 GHz air-couple antenna, and a GSSI 400MHz ground-coupled antenna horn, both antennas are attached to the rear of the vehicle on a retractable frame for easier transportation and deployment. Due to deployment time issues the GPR scans were conducted in August and September of 2021, ideally the FWD and GPR testing would be near identical time frames, but the GPR testing was conducted on relatively warmer days of the months to match the environmental conditions experienced during the FWD testing.

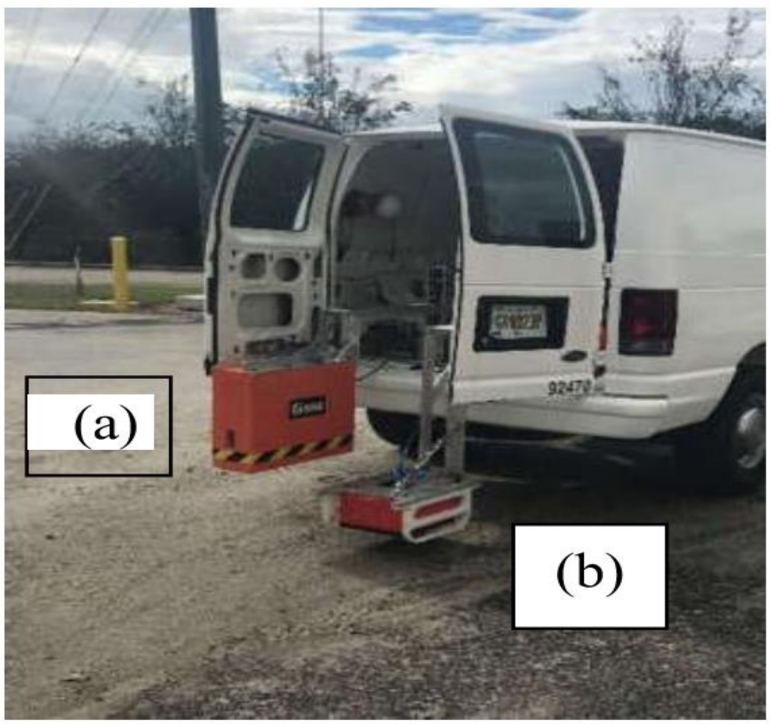

Figure 18: GPR System a) 2 GHz air coupled antenna, b) 400MHz Ground-coupled antenna

3.1.4 GDOT Resilient Modulus Map

With the release of the 1993 AASHTO Design Guide and the recommended changes by utilizing subgrade resilient modulus state agencies had to determine the resilient modulus of their jurisdiction. The current resilient modulus values by GDOT engineers are based upon a series of maps that list subgrade resilient modulus for each county in Georgia based upon historic soil support value (SSV) that were used by the 1972 AAASHTO design guide for flexible pavements. SSV values are determined by soil laboratory testing according to ASTM D1883 *Standard Test Method for California Bearing Ratio (CBR) testing.* Instead of implementing an intensive campaign to gather Mr values, the current map by Kim and Pahno et. al. 2019 was developed which used mathematical models to relate the known SSV values at each county to equivalent Mr values and was validated with limited laboratory testing as seen in Figure 19.

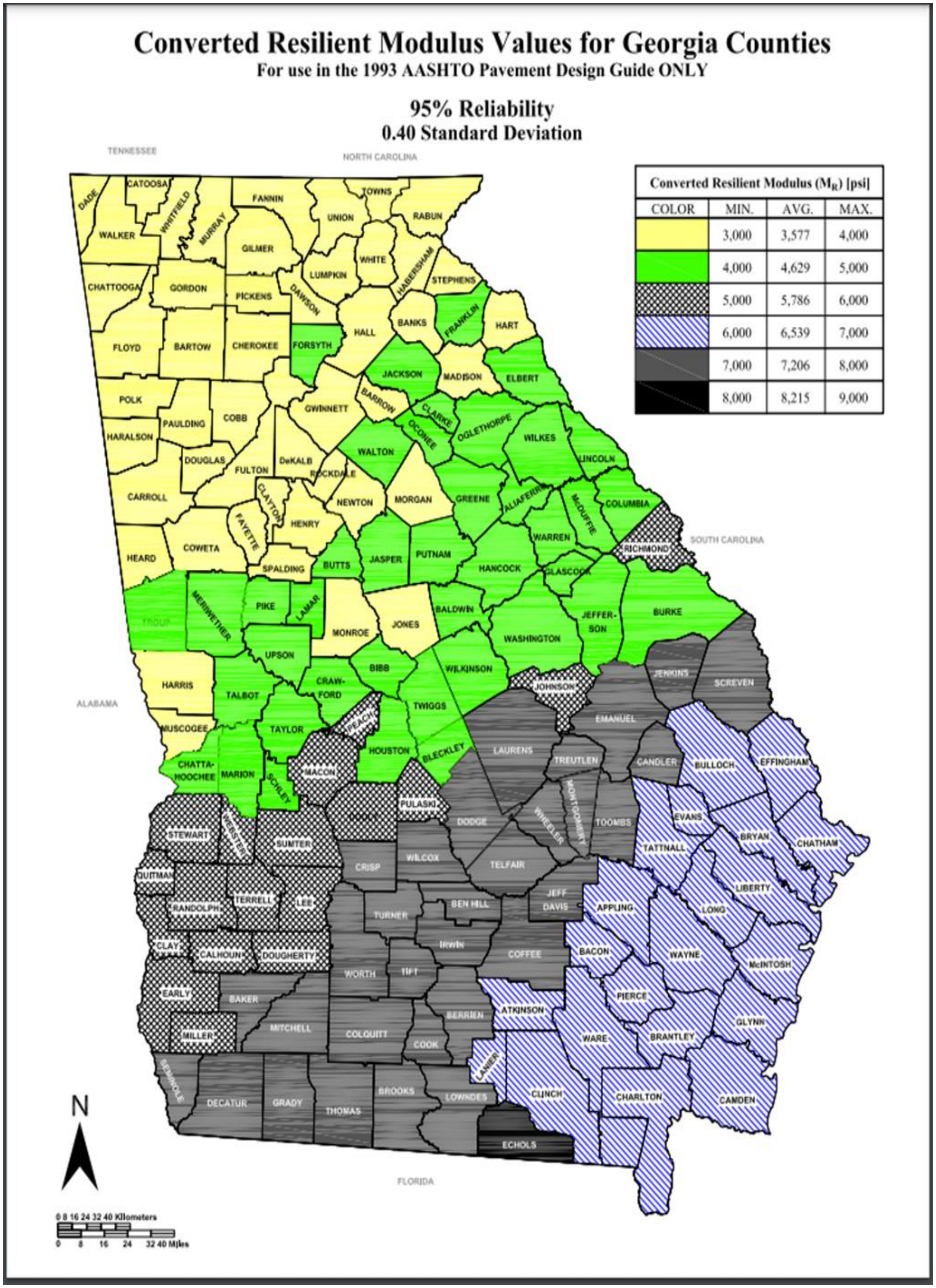

Figure 19: GDOT Resilient Modulus MEPDG Input Map

3.2 Back calculated Resilient Modulus

To obtain the initial resilient modulus data from the FWD testing, the methodologies prescribed in the 1993 AASHTO Pavement Design Guide were used to back calculate the design resilient modulus from the deflection data as formulated below. The AASHTO Mr back calculation method, Equation 3-3 requires the deflection value for a given load at a known distance away from the FWD loading point.

$$\text{Design } M_R = C\left(\frac{0\ 24P}{d_r r}\right) \tag{3-3}$$

Where

Mr = back calculated subgrade resilient modulus, (psi.)

P = applied load, (psi.)

Dr = measured deflection at radial distance r, (inches)

r = radial distance at which the deflection is measured, (inches)

C = 0.33, adjustment factor

However, the raw data cannot be directly used for the back calculation because the deflection load is not exactly at the prescribed 6, 9, or 12-kip and has some variance due to limitations of the FWD testing device. The raw FWD load and deflection data must be normalized to the same load levels to reduce the variance between each testing point. The normalization factor returns the load to the standard load whether 6, 9, or 12-kip and then the raw deflection data is multiplied by the factor to yield a normalized value, as demonstrated in Table 4 below.

Table 4: Example FWD Load Normalization Chart

RAW GPR LOAD (lbf.)	EXAMPLE Deflection (mils.)	*NORMALIZATION FACTOR*	Normalized GPR LOAD (lbf.)	Normailized Deflection (mils.)
5680	0.345178	1.056338028	6000	0.36462465
6110	0.445615	0.981996727	6000	0.43759247
5990	0.412762	1.001669449	6000	0.41345109
6230	0.471648	0.963081862	6000	0.45423563
5770	0.366514	1.039861352	6000	0.38112374
5980	0.401234	1.003344482	6000	0.40257592

With the normalized FWD data the resilient modulus can be back calculated. The GDOT FWD data uses a series of 9 geophones to collect the deflection data within the deflection basin spaced out from the loading point out to 120 inches to pick up deflection data correlated with the resistance by deep subgrade layer stiffness. To determine the resilient modulus of the insitu subgrade, the deflection data associated with the geophone around 36 inches from the loading center (GDOT geophone 6), so the stiffness of the pavement, subbase, and top layer of compacted subgrade are not included in your calculation. With all the input factors classified, the values can be input into the AASHTO equation and yield the FWD back calculated Mr.

The next variable that can be extracted from the FWD testing data is the ISM per station. For this study the only ISM data derived was for the d1(0”), d5(24”), d6(36”), and the d7(60”) geophones. To achieve the ISM data required, the normalized load was divided by the normalized deflection data and the units were converted to fit the AASHTO standard procedures, as demonstrated below.

To ensure there was no anomalous reading within each ISM data set the d1(0”) composite ISM data was plotted against station to ensure that each the 6,9, and 12-kip reading were similar and that there was no error with any of the 6 drops per station. If the ISM is similar amongst the 3 different drops, then there were no data anomalies, and the deflection data can be represented as reliable. The ISM vs. station plot is displayed in Figure 20 for the SR. 10 eastbound lane location and repeated for each section.

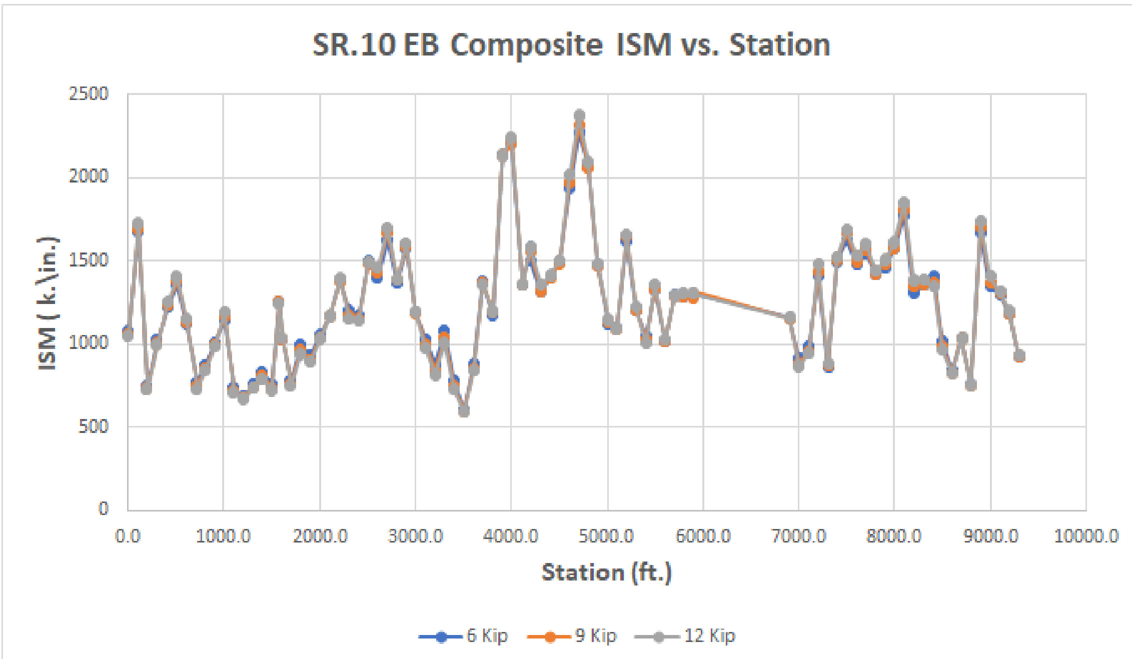

Figure 20: Composite ISM Plot

With the ISM plot created, the individual road sections can be analyzed as separate sections for proper pavement thickness to match the extracted cores from the roadway such as Table 5 and highlight the different areas of investigation.

Table 5: SR 10 Extracted Core Data Sheet

SR 10 Walton County											
County	**Route**	**Lane**	**Direction**	**Core**	**Station**	**MP**	**AC**	**Base**	**Latitude**	**Longitude**	**Notes**
Walton	10	2	Eastbound	1	0.0	2.68	10.75	GAB	33.8301863	-83.866318	Plans suggest 10" GAB, 120334-
Walton	10	2	Eastbound	2	2304.9	3.11	10.50	GAB	33.82959828	-83.85873935	Plans suggest 10" GAB, 120334-
Walton	10	2	Eastbound	3	5301.6	3.68	10.00	GAB	33.82955858	-83.84883209	Plans suggest 10" GAB, 120334-
Walton	10	2	Eastbound	4	8703.2	4.32	10.00	GAB	33.82911551	-83.83759228	Plans suggest 10" GAB, 120334-
Walton	10	2	Westbound	5	0.0	4.45	12.75	GAB	33.82926218	-83.83558124	Plans suggest 10" GAB, 120334-
Walton	10	2	Westbound	6	3318.1	3.83	13.00	PCC	33.8296943	-83.84653504	Unable to recover PCC, Plans suggest 9 inches
Walton	10	2	Westbound	7	6003.6	3.32	11.00	GAB	33.82960165	-83.85542191	Plans suggest 10" GAB, 120334-
Walton	10	2	Westbound	8	8502.0	2.84	14.75	PCC	33.83020733	-83.86365197	Unable to recover PCC, Plans suggest 9 inches
Walton	10	1	Eastbound	9	0.0	2.70	10.50	GAB	33.83020231	-83.86587621	Plans suggest 10" GAB, 120334-
Walton	10	1	Eastbound	10	3201.0	3.31	11.25	GAB	33.82942659	-83.85533724	Plans suggest 10" GAB, 120334-
Walton	10	1	Eastbound	11	6902.7	4.01	10.00	GAB	33.82938457	-83.84309808	Plans suggest 10" GAB, 120334-
Walton	10	1	Eastbound	12	8901.3	4.39	10.25	GAB	33.82912196	-83.83648652	Plans suggest 10" GAB, 120334-
Walton	10	1	Westbound	13	0.0	4.44	11.50	GAB	33.82921115	-83.83548675	Plans suggest 10" GAB, 120334-
Walton	10	1	Westbound	14	3001.2	3.87	10.00	Soil-Aggregate	33.82959864	-83.84539348	Core showed bottom-up cracking
Walton	10	1	Westbound	15	6309.1	3.25	10.00	GAB	33.82959386	-83.85633691	Plans suggest 10" GAB, 120334-
Walton	10	1	Westbound	16	8601.7	2.81	9.25	PCC	33.83017357	-83.86390271	Unable to recover PCC, Plans suggest 9 inches

3.3 Determining Traffic Inputs

The FWD back calculated Mr based upon the AASHTO 1993 procedures will be compared to the values of the currently implemented resilient modulus map. Both Mr values will be implemented to design a flexible pavement section based upon known traffic loading conditions and other GDOT flexible pavement design methodologies. To obtain an accurate representation of the current, existing traffic loading conditions at each roadway site, the GDOT Traffic Analysis and Data Application (TADA) will be utilized, as demonstrated below.

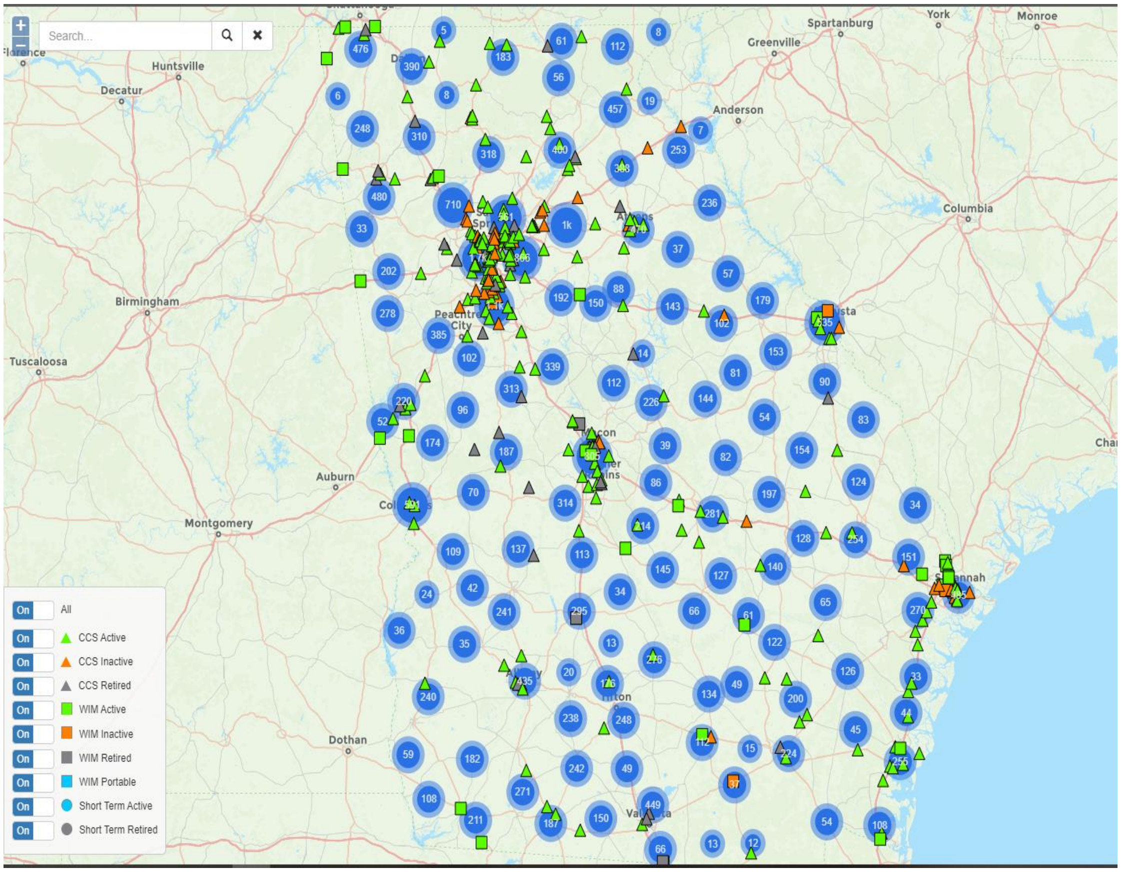

Figure 21: GDOT TADA System

The TADA system gathers, stores, and displays traffic counts based upon average annual daily traffic (AADT) and breaks it down with percent truck data and further into single unit (SU) and multiunit (MU) average annual daily truck traffic (AADTT). GDOT uses both actual and estimated traffic volumes for each location and is dependent on the needs and abilities of each district office. Also, every site has a detailed breakdown of the vehicle types encountered and includes several time and date distributions, site metadata, and as shown in Figure 22.

Figure 22: TADA Site Specific Data

To determine the ESAL factor experienced at each testing location for designing pavement sections the data for that roadway and any active and actual AADTT values were synthesized in the TADA system and recorded. To simply the ESAL calculation, the average for each section was taken and utilized in the pavement design calculations, as highlighted in the next chapter.

CHAPTER 4 DATA ANALYSIS

4.1 GPR Survey Results

The first step of the data ingestion process was reviewing the extracted cores provided by GDOT and compare to the results of the GPR scans for depth measurements. The cores provided initial information regarding roadway stratification, base and subbase layers, and roadway health. Out of the 9 roadways investigated, 7 of the routes had at least 4 cores per section, with SR 10 having 15 and SR 57 in Emmanuel County had less than 3 cores available due to the condition of the roadway and the extensive cracking and noted crumbing of the extracted cores from that section. After reviewing the Emmanuel County core, the GPR scan and video files highlighted that the section had been repaved after the core was extracted so, the GPR data was not considered for this study due to the replacement of the roadway. However, the FWD data that was captured at the same time of the core extract on noted the poor health of the roadway as well, so the FWD data for the SR 57 section in Emmanuel County was also not considered for this report.

The FWD and GPR data for the SR 26 section in Bulloch County was also not considered because upon the review of the extracted cores the pavement was less than 4.50 inches of asphalt laid upon 6 inches of Portland cement concrete (PCC), which requires different back calculation methods and behaves differently than the other flexible pavement sections of the investigation.

To verify the roadway thickness in between the extracted cores, the GPR scan data was filtered for drastic change in polarity to identify the boundary between the air, asphalt, subbase, and subgrade layers as Figure 21 shows, with depth along the y-axis and the station along the x-axis.

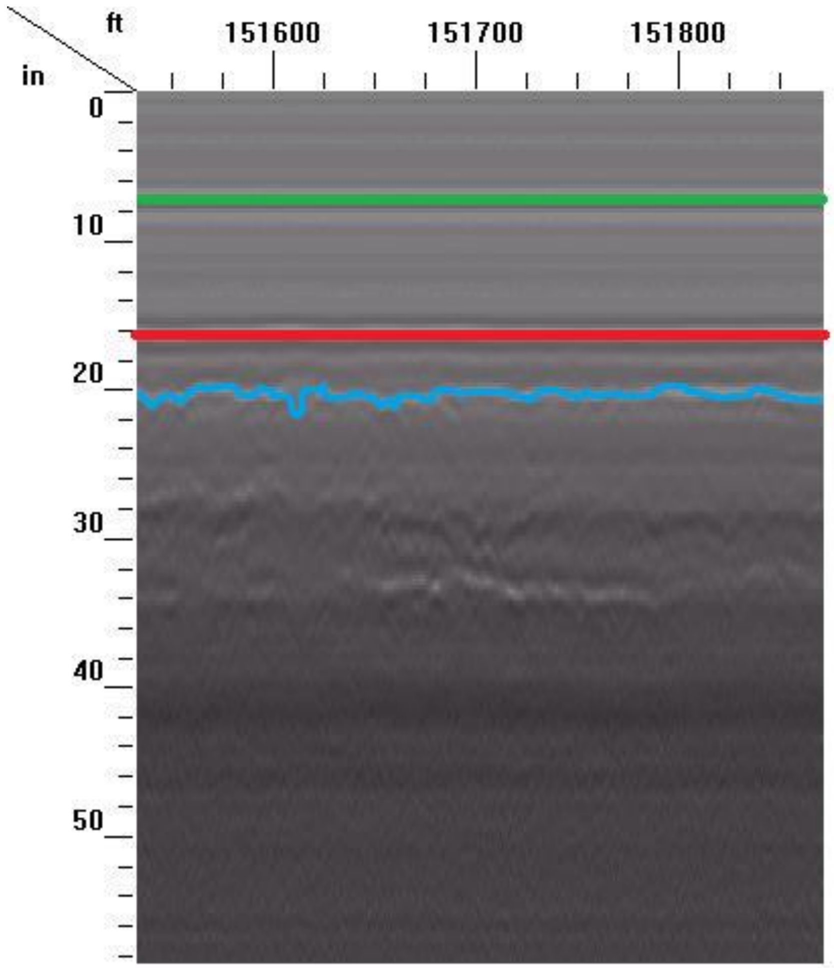

Figure 23: Raw GPR Results

When visually interpreting raw GPR data, the change in polarity of the return signal, or change of line color from black and white indicates a change of material type. In roadway GPR scans, the change of layers from air, pavement, GAB, and subgrade are typically very strong signals due to the layered construction of the roadway section.

GSSI has several algorithms to auto calculate the depth of each high polarity change as noted by a sharp change in color, again, typically from black to white. The GSSI program noted 4 separate layers in the above GPR scan result, with the air-asphalt boundary line as a solid, smooth green line around 8-inch depth marker, which is the distance from the bottom of the air-coupled horn deployed from the GPR vehicle to the roadway surface. Next, the asphalt-subbase interaction line as seen around the solid red line at the 16-inch depth marker. Lastly, the subbase-subgrade interaction line in noted as an increase of noise visualized as a series of sharp parabolic curves underneath the roadway, as highlighted by the solid blue line at the 20-inch depth marker. The program captures the layers depth as designated by the previously mentioned polarity change and is visually verified throughout the section image results, the results of this processing were then record. To confirm the results of the GPR scans the determined thickness was compared to the measured depth of the cores extracted by GDOT, which confirmed the GPR was determining the accurate roadway depth.

Next, the GPR amplitude data was compared to a copper sheet at the beginning of each scan to relate the GPR response and determine the dielectric constant of the road and subgrade stratification. The determined dielectric constant was then inserted into the previously highlighted subgrade density model resulting in the estimated subgrade density. All the GPR data for the subgrade and roadway were recorded and summarized in a Table 6 and Table 7, respectfully.

Table 6: GPR SR 10 Soil Data Summary

GPR-Summary Data					
Scan	Distance (ft)	Distance (mi)	subgrade γ_{dry} (pcf)	Layer 3 Dielectric	W.C.
0	0.00	0.00	89.62	5.87068	0.101
1	0.64	0.00	92.35	7.11797	0.11
2	1.28	0.00	101.09	13.1403	0.13
3	1.92	0.00	94.04	8.02745	0.115
4	2.56	0.00	84.39	4.07912	0.082
5	3.20	0.00	82.94	3.6944	0.076
6	3.84	0.00	78.81	2.78165	0.055
7	4.48	0.00	85.35	4.35883	0.086
8	5.12	0.00	85.32	4.35068	0.086

Table 7: GPR SR 10 Roadway Data Summary

Scan	Distance (ft)	Distance (mi)	subgrade density (pcf)	Asphalt layer thickness (in.)
0.000	0.000	0.000	89.620	14.530
1.000	0.640	0.000	92.346	14.180
2.000	1.280	0.000	101.091	14.530
3.000	1.920	0.000	94.043	14.530
4.000	2.560	0.000	84.387	14.870
5.000	3.200	0.001	82.943	14.870
6.000	3.840	0.001	78.814	15.220
7.000	4.480	0.001	85.350	15.220
8.000	5.120	0.001	85.323	15.910

4.2 Resilient Modulus Back calculation

The next step was to ingest the GDOT FWD dataset and tabulate all the desired values necessary for subgrade resilient modulus back calculation. The raw data from GDOT is listed in the Appendix at the end of the report. The deflection values and drop values were normalized to 6,9, and 12-kip loads with their adjusted deflections as well. Next, the resilient modulus was back calculated with the normalized values, and in a separate column the adjustment factor, C=0.33 was incorporated yielded the result titled, 'Factored Mr', as demonstrated in the table below and repeated for each normalized load and section.

<u>Table 8: SR. 10 Eastbound '93 AASHTO Mr Back calculation Results</u>

9kip - SR10 EB Resilient Modulus			
STATION (ft.)	Force (lbs.)	Mr (36) (psi.)	Factored Mr (36)
0.0	9000.0	17367	5731
0.0	9000.0	17461	5762
101.1	9000.0	28366	9361
101.1	9000.0	28717	9477
197.3	9000.0	12244	4041
197.3	9000.0	12016	3965

With the factored Mr values known, the resulting resilient modulus values were taken and the ISM, d (0'') sensor, for each load and section were determined in Table 5 and plotted in Figure 20. The ISM plot ensures that there are no inconsistencies in the data or calculation methods, as the yielded ISM per drop at each station should be relatively similar. Also, the ISM plot is helpful in identifying areas of similar pavement performance for determining structural number based upon pavement thickness or other common structural parameter of that section of the roadway. The ISM versus station plots highlighted areas of discontinuity not noted in the Mr back calculated values.

Table 9: SR 10 Eastbound FWD-GPR Data Sheet

SR 10 EB FWD-GPR Data									
STATION (ft.)	STATION (ft.)	Factored Mr (36) (PSI.)	Selected Mr (36) (PSI.)	subgrade density (pcf)	Layer 3 Dielectric	DEFL d6(36")	SEL. DEFL d6(36")	ISM_d1 (k./in.)	SEL. ISM_d1
0		13247				1.51		877.61	
0	0	13371	13247	93.84	11.84	1.49	1.51	877.52	877.61
104.8		11420				1.75		884.52	
104.8	104.8	11467	11420	79.67	4.02	1.74	1.75	888.25	884.52
209.7		14677				1.37		929.81	
209.7	209.7	14843	14677	91.63	10.03	1.35	1.37	926.55	929.81
301.7		10730				1.86		860.72	
301.7	301.7	10532	10730	90.8	9.42	1.89	1.86	861.71	860.72
407.4		12244				1.63		948.95	
407.4	407.4	11440	12244	81.78	4.72	1.74	1.63	937.62	948.95
497.4		10679				1.86		800.44	
497.4	497.4	10645	10679	80.94	4.43	1.86	1.86	802.85	800.44
613.8		9351				2.13		737.21	
613.8	613.8	9104	9351	87.47	7.3	2.18	2.13	735.81	737.21

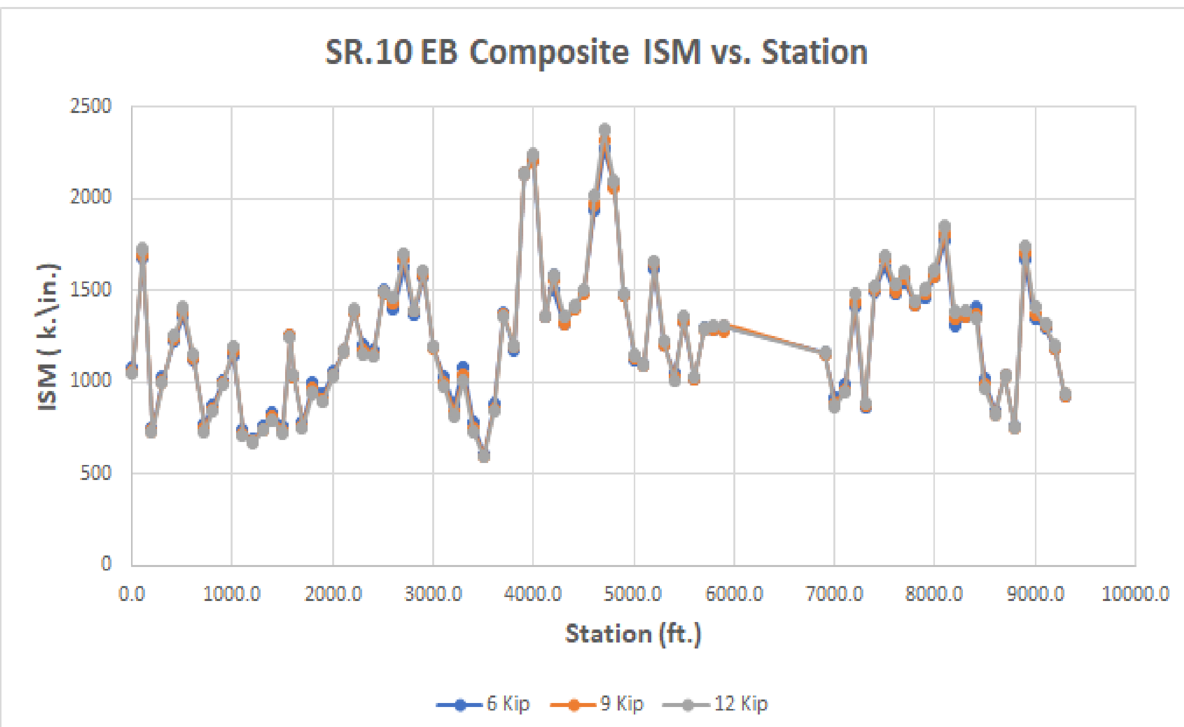

Figure 24: SR10 Eastbound ISM Plot

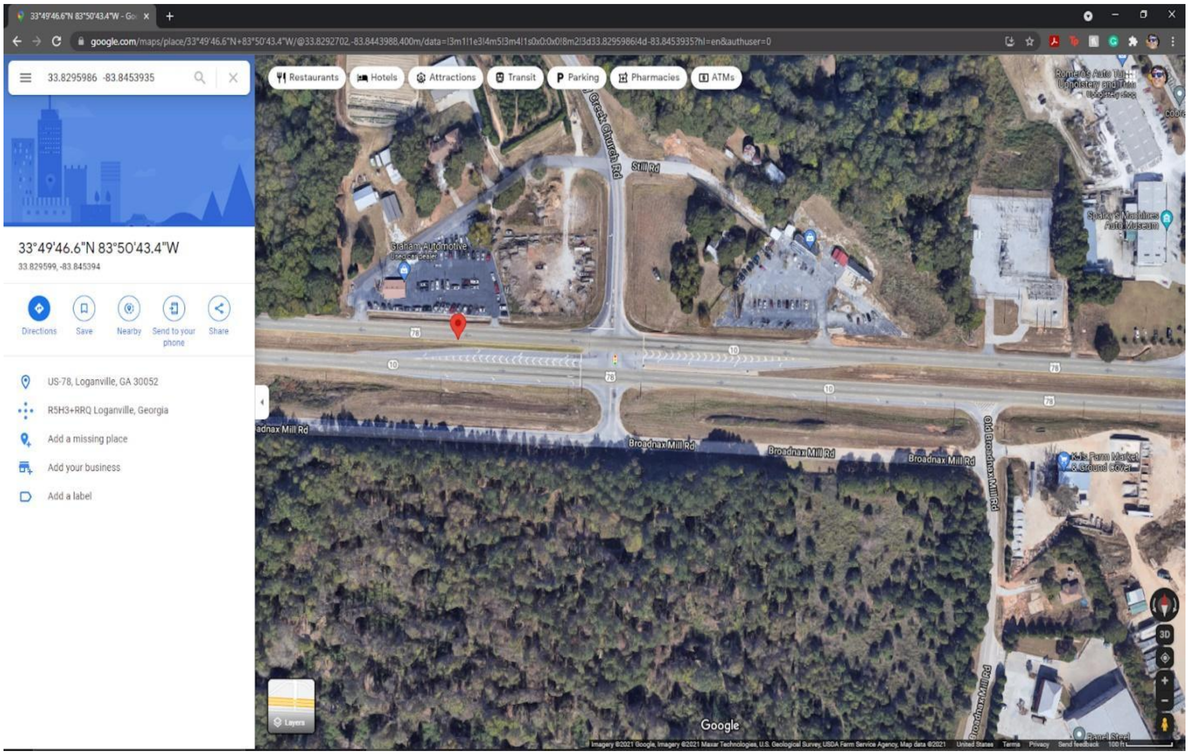

Figure 25: Satellite Image of Anomalous Site

Figure 24 for SR 10 EB can estimate as 3 different sections with section one spanning station 0-3500 feet, section 2 from 3500-6000 feet, and section 3 as the span from 6000-9300 feet. Note, the road has extended intersection from station 6000-7000 feet highlighted in Figure 25, so now FWD data could be acquired from this section. This similar process was conducted for the other 8 sections of the investigation.

With the resilient modulus of each section determined, and a corresponding ISM plot graphed, the back calculated Mr values will be compared to the GDOT implemented resilient modulus values determined from laboratory testing. A statistical analysis of the resilient modulus data for each section was conducted and tables were formed as demonstrated below:

Table 10: SR 10 EB Resilient Modulus Statistical Overview

SR 10 (Walton County)	
Resilient Modulus (psi.)	
Mean	7190
Standard Error	296
Median	6819
Mode	#N/A
Standard Deviation	2749
Sample Variance	7555272
Kurtosis	0
Skewness	0
Range	11921
Minimum	2647
Maximum	14568
Sum	618365
Count	86
Confidence Level(95.0%)	589

Table 11: SR 82 EB Resilient Modulus Statistical Overview

SR 82 (Jackson County)	
Resilient Modulus (psi.)	
Mean	6457
Standard Error	370
Median	5989
Mode	#N/A
Standard Deviation	3263
Sample Variance	10649793
Kurtosis	2
Skewness	1
Range	15886
Minimum	1532
Maximum	17418
Sum	503661
Count	78
Confidence Level(95.0%)	736

The eastbound SR10 and SR 82 descriptive statistics both indicate the high variability of the back calculated resilient modulus values with minimums and maximums significantly outside the bounds of the GDOT prescribed values from the previously mentioned resilient modulus map leading to a high standard deviation. Next, a 95% confidence interval is calculated according to equation 3-4 for each target roadway section and was used to determine the range of values for the mean resilient modulus value and used for AASHTO roadway design procedures.

$$CI = \mu \pm z\frac{\sigma}{\sqrt{n}} \tag{3-4}$$

Where:

CI = Confidence Interval

μ = Sample Mean

z = Confidence Level Value

σ = Sample Standard Deviation

n = Sample Size

4.3 Effect of Resilient Modulus on Pavement Design

With the FWD back calculated subgrade resilient modulus determined for all sections of the investigation, the effect of the perceived change of the resilient modulus was to be determined by comparing the results of AASHTO 1993 new section pavement design calculations. To calculate the change in pavement the TADA traffic data was combined with the average GPR asphalt pavement thickness, and the FWD back calculated resilient modulus were combined and summarized in Table 12.

Table 12: Flexible Design Summary Data

LOC (SR)	Subgrade Information			Traffic Information			Traffic Information		
	Mr 36 (psi.)	Map (95% Conf)	[FWD - Map] Mr (psi)	AADT	SU	MU	ASUT	AMUT	20Y-ESAL
10	6600 - 7780	4,629	*1971 - 3151*	20,000	1,300	1,000	189,800	547,500	14,746,000
11	6825 - 8525	4,629	*2196 - 3896*	11,000	700	800	102,200	438,000	10,804,000
22	7733 - 9580	4,629	*3104 - 4951*	4,000	200	500	29,200	273,750	6,059,000
57	12550 - 20680	5,786	*6764 - 14894*	2,000	200	600	29,200	328,500	7,154,000
73	10562 - 13108	6,539	*4023 - 6569*	7,000	500	600	73,000	328,500	8,030,000
82	5721 - 7193	4,629	*1092 - 2564*	5,000	300	250	43,800	136,875	3,613,500
129	5787 - 6663	7,206	*(-1419) - (-543)*	1,600	200	200	29,200	109,500	2,774,000

To simply the flexible pavement design calculations a spreadsheet was used based upon the nomograph associated with the AASHTO design guide. The same roadway cross section minimum requirements, traffic data, and GDOT flexible pavement coefficients were implemented but two iterations were conducted per section with the first utilizing the GDOT map for subgrade resilient modulus input and the second used the previously calculated FWD back calculated resilient modulus values.

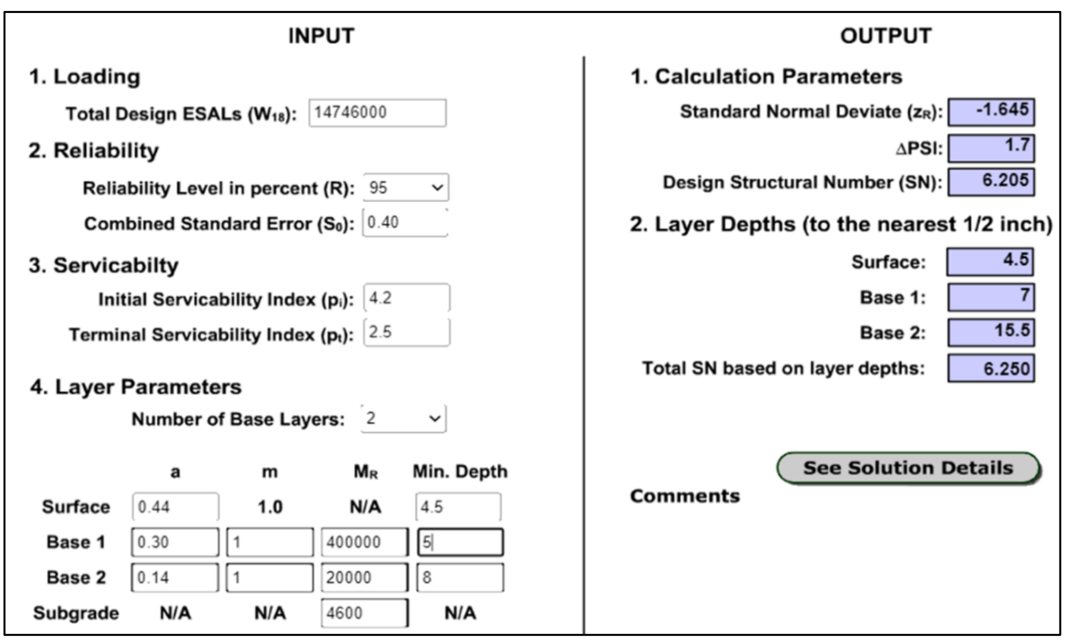

Figure 26: Map Flexible Design Output

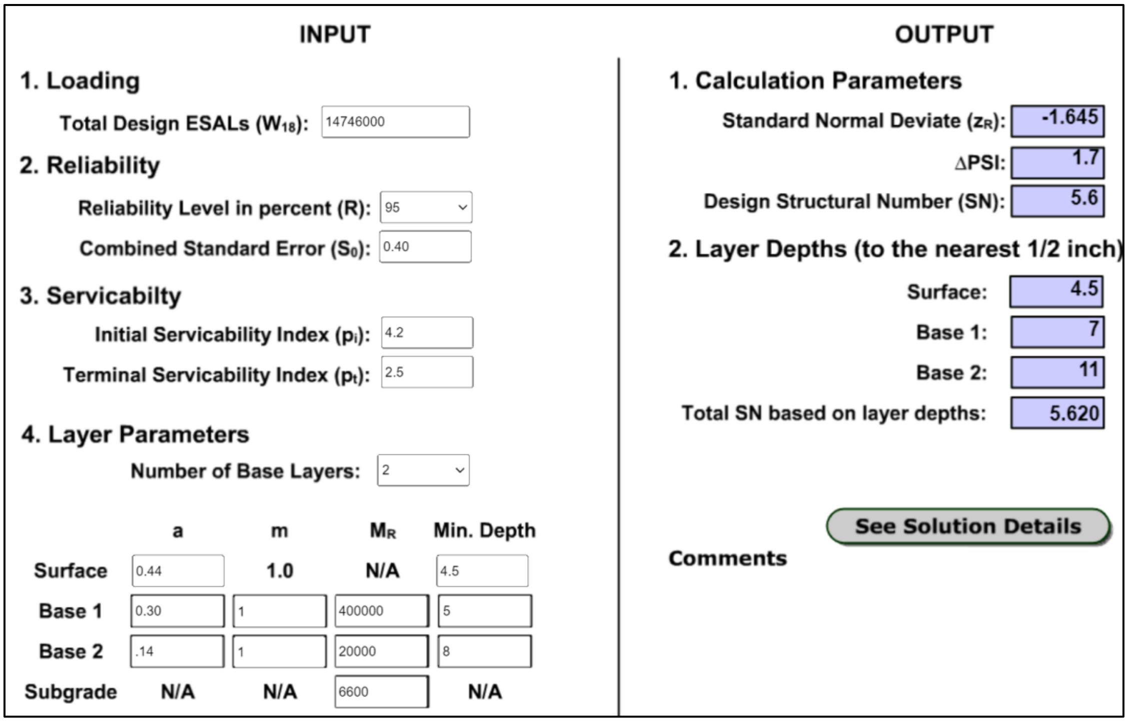

Figure 27: FWD Flexible Design Output Lower Bound

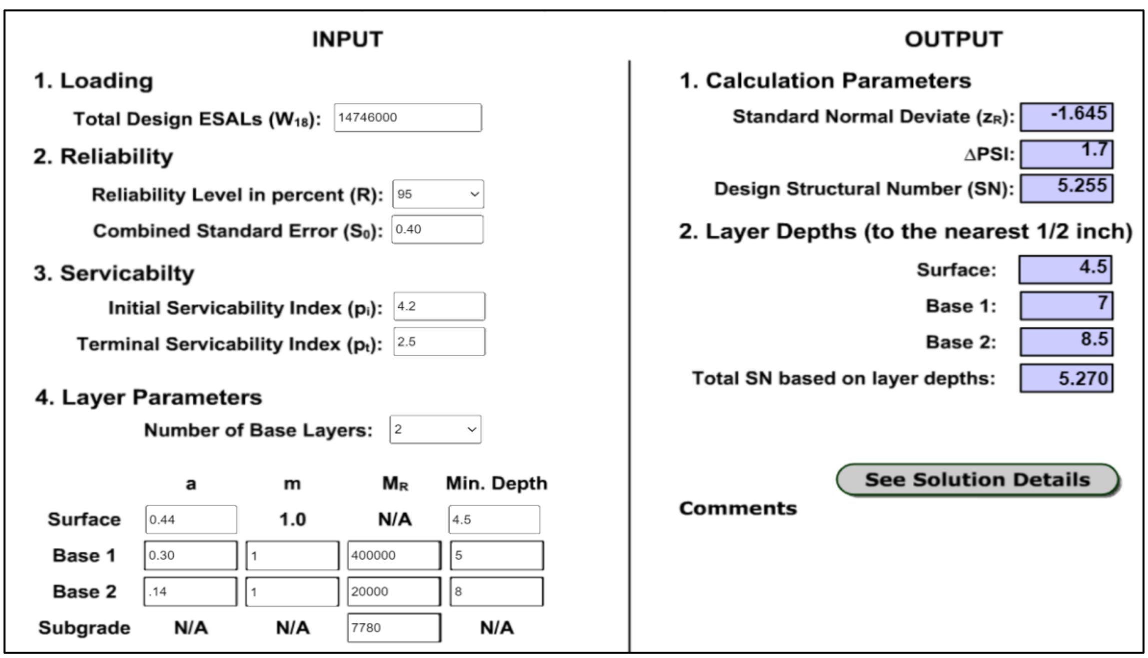

Figure 28: FWD Flexible Design Output Upper Bound

As shown by the Figure 27 and Figure 28, the structural number (SN) for the FWD back calculated resilient modulus roadway section was 0.63 to 0.98 lower the structural number required based upon the Map subgrade Mr value. The given spreadsheet increased the granular aggregate base (GAB) layer thickness but maintained the same asphalt layer thickness. Typically, GDOT uses 8 inches of GAB for sandy subgrade layers and 12 inches for clayey subgrade, so to maintain with GDOT design practices the layer thickness must be recalculated to maintain the same GAB layer, but reduce the asphalt layer thickness, resulting in a thinner and thus cheaper pavement section. This flexible design calculations were conducted for the results of each pavement section and listed in the summary in Table 13.

Table 13: Flexible SN Summary Output

SR	Map Mr (psi.)	FWD Mr (psi.)	δ SN (#)	δ AC (in.)	Rounded δ AC (in.)	GENERAL NOTES
10	4,629	6600 - 7780	0.63 - 0.98	2.10 - 3.25	2.25 - 3.25	Reduction in AC possible
11	4,629	6825 - 8525	0.70 -1.05	2.33 - 3.50	2.50 - 3.50	Reduction in AC possible
22	4,629	7733 - 9580	0.84 - 0.98	2.80 - 3.25	3.00 - 3.25	Reduction in AC possible
57	5,786	12550 - 20680	0.49*	1.63	1.75	No change in SN with FWD-Mr range
73	6,539	10562 - 13108	0.42*	1.40	1.50	No change in SN with FWD-Mr range
82	4,629	5721 - 7193	0.35 - 0.77	1.16 - 2.56	1.25 - 2.75	Reduction in AC possible
129	7,206	5787 - 6663	(-0.28) - (-0.07)	(+.93) - (+.23)	(+1.00) - (+0.25)	Additional AC required

SR 10,11,2121,57,73, and 82 resulted in thinner pavement sections and SR 129 in Candler County resulted in a thicker pavement requirement. The resilient modulus was estimated via the SSV method to have the stiffest subgrade, but the FWD back calculation method resulted in a lower subgrade resilient modulus value. The change in result of the Candler County subgrade could provide insight into the accuracy of SSV to Mr model at higher SSV values, but there were not enough roadway sections in the investigation to develop any hypothesis on the subgrade resilient modulus outcome phenomenon.

4.4 Cost Estimation of Pavement Change

To further determine the impact of increased resilient modulus values on roadway design an economic impact consideration will be reviewed based upon GDOT 2012-unit cost data for jobsite practices and materials. As the table below demonstrates, the item/practice, unit of measure, and weighted average unit cost across all jobsites during the reported timeframe is listed.

Table 14: 2012 GDOT Unit Cost Fact Sheet

ITEM CODE	ITEM DESCRIPTION	QUANTITY	USE	UM	MEAN	WTD AVG
310-5080	GR AGGR BASE CRS, 8 INCH, INCL MATL	51,553.00	12	SY	13.60	13.51
310-5100	GR AGGR BASE CRS, 10 INCH, INCL MATL	8,108.00	3	SY	26.67	18.53
310-5120	GR AGGR BASE CRS, 12 INCH, INCL MATL	78,558.00	7	SY	20.21	18.39
310-5140	GR AGGR BASE CRS, 14 IN, INCL MATL	17,389.00	1	SY	17.25	17.25
318-3000	AGGR SURF CRS	44,421.60	54	TN	20.37	17.36
400-3150	ASPH CONC 9.5 MM OGFC, GP 2 ONLY, INCL POLY-MOD., BIT. MATERIAL AND H LIME	526.00	1	TN	130.62	130.62
400-3206	ASPH CONC 12.5 MM OGFC, GP 2 ONLY, INCL POLYMER-MODIFIED BITUM MATL & H LIME	36,540.00	3	TN	95.90	96.00
400-3624	ASPH CONC 12.5 MM PEM, GP 2 ONLY, INCL POLYMER-MODIFIED BITUM MATL & H LIME	157,945.00	4	TN	103.80	106.30
402-1802	RECYCLED ASPH CONC PATCHING, INCL BITUM MATL & H LIME	105,394.00	55	TN	111.99	77.35
402-1812	RECYCLED ASPH CONC LEVELING, INCL BITUM MATL & H LIME	353,160.00	170	TN	78.27	71.77
402-3100	RECYCLED ASPH CONC 9.5 MM SUPERPAVE, TYPE I, GP 1 OR BLEND 1, INCL BITUM MATL & H LIME	254,595.00	67	TN	75.52	72.87
402-3101	RECYCLED ASPH CONC 9.5 MM SUPERPAVE, TYPE I, BLEND 1, INCL BITUM MATL & H LIME	107,557.00	43	TN	74.93	71.74
402-3102	RECYCLED ASPH CONC 9.5 MM SUPERPAVE, TYPE II, BLEND 1, INCL BITUM MATL & H LIME	143,234.00	23	TN	72.16	67.49
402-3103	RECYCLED ASPH CONC 9.5 MM SUPERPAVE, TYPE II, GP 2 ONLY, INCL BITUM MATL & H LIME	155,405.00	39	TN	82.51	73.73
402-3113	RECYCLED ASPH CONC 12.5 MM SUPERPAVE, GP 1 OR 2, INCL BITUM MATL & H LIME	47,576.00	3	TN	69.26	68.29
402-3121	RECYCLED ASPH CONC 25 MM SUPERPAVE, GP 1 OR 2, INCL BITUM MATL & H LIME	565,418.50	60	TN	77.91	65.04
402-3130	RECYCLED ASPH CONC 12.5 MM SUPERPAVE, GP 2 ONLY, INCL BITUM MATL & H LIME	430,609.10	69	TN	83.63	72.65
402-3147	RECYCLED ASPH CONC 12.5 MM SUPERPAVE, BLEND 1, INCL BITUM MATL & H LIME	371.00	1	TN	64.34	64.34
402-3190	RECYCLED ASPH CONC 19 MM SUPERPAVE, GP 1 OR 2,INCL BITUM MATL & H LIME	274,992.40	77	TN	84.11	67.49

As shown in Table 14, line-item code #400-3624 the 12.5(mm) asphalt concrete with polymer binder has a weighted average of $106.30/ton. Which is roughly $42,000 per inch of pavement thickness, per lane mile, assuming typical asphalt pavement unit weight of 150 (lbs/ft^3). This economic analysis shows that using a thicker pavement is a more conservative structural design but leads to excessive cost incurred due to the excess material alone.

4.5 Resilient Modulus Prediction Models

Due to the overestimate and the high variability of the FWD back calculated Mr value compared to the AASHTO 1993 prescribed resilient modulus calculation, the collected field data was applied to other Mr prediction models to better describe the insitu subgrade values. The first prediction model was derived from the dielectric constant values extracted from the GPR dataset. The subgrade dielectric constant was determined from the previously mentioned GPR density model where the normalized reflections are compared, and a dielectric constant value is determined. Since the value provides continuous insitu values, the output response will have more significant impact on Mr prediction than FWD back calculation methods. The dielectric constant values were plotted against the FWD back calculated Mr value to determine if a relationship exists and the graph is highlighted below.

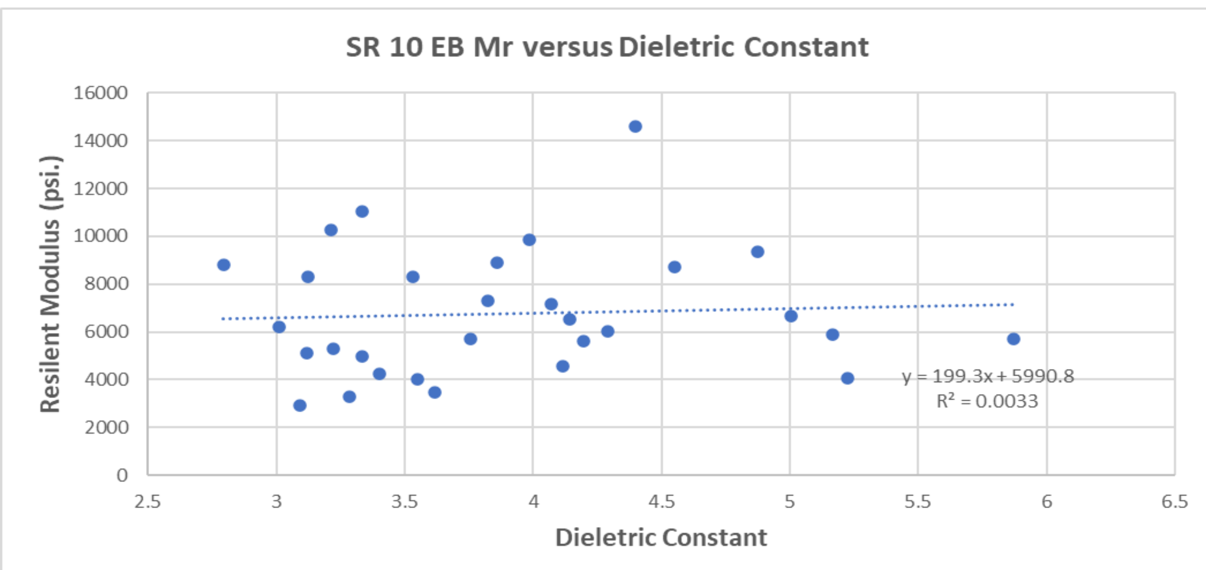

Figure 29 : SR 10 EB Resilient Modulus versus Dielectric Constant

As demonstrated in Figure 29 above, a linear model with an R^2=0.0033, there is no direct correlation between the two values, so a multilinear regression model is necessary, which is parallel with previous resilient modulus prediction models.

A linear regression model was derived from dielectric constant to predict the resilient modulus, since it can provide insight into water content, density, and porosity all which relate to the resilient modulus of the roadway subgrade. However, the linear regression model yielded low (R^2=0.001) correlation values as shown in Table 15:

Table 15: Initial Linear Regression Model Output

Regression Statistics								
Multiple R	0.032							
R Square	0.001							
Adjusted R Square	-0.036							
Standard Error	2787.002							
Observations	86							
ANOVA								
	df	*SS*	*MS*	*F*	*Significance F*			
Regression	3	656441	218814	0.0282	0.9936			
Residual	82	636925201	7767380					
Total	85	637581642						
	Coefficients	*Standard Error*	*t Stat*	*P-value*	*Lower 95%*	*Upper 95%*	*Lower 95.0%*	*Upper 95.0%*
Intercept	62409.77	309627.88	0.2016	0.8408	-553538.73	678358.27	-553538.73	678358.27
X Variable 1	-822.02	4588.54	-0.1791	0.8583	-9950.08	8306.04	-9950.08	8306.04

Next, the derived density model based off the dielectric constant value and water content was compared to the Mr values for the development of a prediction model. The density value and Mr was directly compared, and the resulting plot is highlighted below. Note, the spread of the data, where no regression equation could be applied with reasonable results.

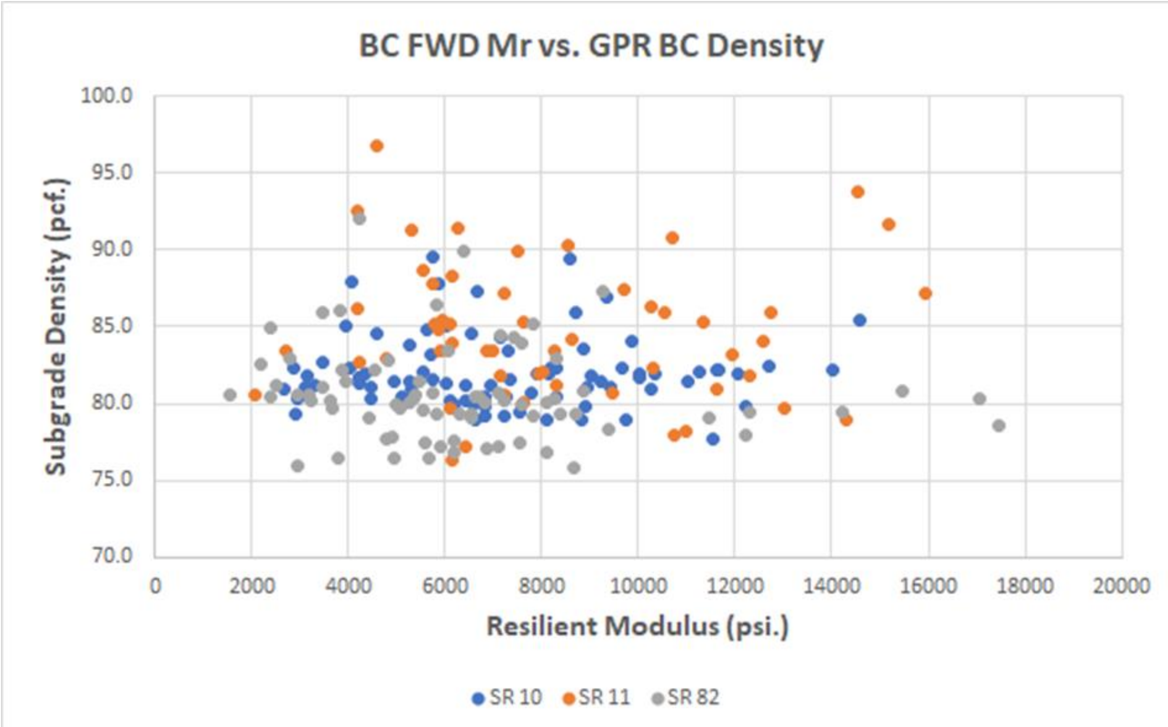

Figure 30: Combined Section Subgrade Mr versus Density

Lastly, a basic resilient modulus prediction power model with dielectric constant as an input, in the form $Mr = \alpha(X)^{\beta}$ that was based off an error reduction solver, however this also yielded low R^2 correlation values as well. Since none of the prediction models yielded credible results, further investigation is required to link any of the GPR and FWD data, at this time.

CHAPTER 5 CONCLUSIONS

This study details the investigation of back calculating subgrade resilient modulus from current GDOT Falling Weight Deflectometer procedures from project sites around the state. The back calculation methodology follows the prescribed procedures in the AASHTO 1993 Pavement Design Guide based upon field deflection testing.

The main research objective was to back calculate the resilient modulus from FWD testing, develop a map of the resilient modulus data, and compare it to previously constructed resilient modulus data maps based upon laboratory testing resilient modulus values. The FWD based Mr map would then be utilized as input parameters for MEPDG procedures.

- The FWD Mr map was compared to the lab testing Mr values and descriptive statistical analysis was conducted to determine the validity of the FWD Mr values despite the overall values from the FWD back calculated were higher than the laboratory testing results.
- The reduction in required Structural number due to increased subgrade stiffness led to resulting thinner pavement sections resulting in $42,000 in savings per inch of asphalt per mile of roadway.
- The GPR data was used to capture continuous ground condition data to validate the roadway thickness compared to extracted core and initialize the development of a Mr prediction model based upon the GPR dielectric constant.

CHAPTER 6 RECOMMENDATIONS

With an initial analysis of the data for the 9 roadway sections some recommendations for further study and areas of deeper investigation that is required will be highlighted. Overall, the study highlighted the importance of network level FWD testing is required to fully compare the SSV based resilient modulus to the FWD back calculated resilient modulus values. Several portions of clayey-sand soils in the piedmont region demonstrated promising results, but an emphasis on roadway sections in both north Georgia which has weaker silty soils and South Georgia along the coastline with stiffer sandy subgrade is required due to some inconsistencies in results of the investigation.

To accelerate the implementation of a statewide or network level update to subgrade resilient modulus a machine learning based prediction algorithm on GPR data can continued to be implemented, since FWD testing is significantly more expensive and time consuming versus GPR scanning procedures.

CHAPTER 7 REFERENCES

1. Abdelmawla, A.M. and Kim, S.H. (2021). Use of Ground Penetrating Radar Technology to Assess and Monitor Pavement Structural Conditions for Improved Pavement Maintenance and Rehabilitation Strategies.
2. American Association of State Highway and Transportation officials (AASHTO). (1993). *Guide for Design of Pavement Structures*. Washington, D.C.
3. American Association of State Highway and Transportation officials (AASHTO). (2014). *A Century of Achievement for a Better Tomorrow*. Washington, D.C.
4. American Association of State Highway and Transportation officials (AASHTO) (2021). AASHTO T307-99. Standard Method of Test for Determining the Resilient Modulus of Soils and Aggregates Materials. Washington, D.C. Available at: astm.org/
5. American Society for Testing and Materials (ASTM) (2018). ASTM D6951. Standard Test Method for Use of the Dynamic Cone Penetrometer in Shallow Pavement Applications Washington, D.C. Available at: astm.org/
6. Dinoe A. (2015). Implementation of Resilient Modulus – CBR relationship in Mechanistic-Empirical(M-E) Pavement Design. Cheikh Anta Diop University, Dakar.
7. Federal Highway Administration (FHWA), US. Department of Transportation (2017). *Using Falling Weight Deflectometer Data with Mechanistic-Empirical Design and Analysis, Vol1: Final Report*. Washington, D.C.
8. George, K.P. Falling Weight Deflectometer for Estimating Subgrade Moduli, Report No. FHWA/MS-DOT-RD-03-153, Submitted to Mississippi Department of Transportation, Jackson, MS, 2004.

9. Heuekelom W. and Foster (1960). “Dynamic Testing of Pavement”. ASCE, Journal of the Structure Division No. SM 1, 86.
10. Hossain, M.S. (2009). Characterization of Subgrade Resilient Modulus for Virginia Soils and Its Correlation with the Results of Other Soil Tests, Report No. VTRC 09-R04, Submitted to Virginia Transportation Research Council, Charlottesville, VA.
11. Hossain, M. S., & Apeagyei, A. K. (2010). *Evaluation of the lightweight deflectometer for in-situ determination of pavement layer moduli*: Final report. Virginia Transportation Research Council, Charlottesville, VA.
12. Hossain and Kim Y. (2014). *Estimation of Subgrade Resilient Modulus Using the Unconfined Compression Test*. Virginia Center for Transportation Innovation and Research. Charlottesville, VA.
13. Joshi S. and Malla R. (2009). Subgrade Resilient Modulus prediction models for coarse and fine-grained soils based on long-term pavement performance data. Submitted to International Journal of Pavement Engineering.
14. Kim, S.H. (2004). Determination of Aggregate Physical Properties and Its Effect on Cross-Anisotropic Behavior of Unbound Aggregate Materials. Ph.D. Dissertation, Texas A&M University, College Station, TX.
15. Kim S.H, D. N. Little, and E. Tutumluer, (2007). Effect of Gradation on Nonlinear Stress-Dependent Behavior of a Sandy Flexible Pavement Subgrade, Journal of Transportation Engineering, Volume 133, Issue 10, 2007, pp. 582-589.
16. Kim S.H. (2013). *Measurements of Dynamic and Resilient Moduli of Roadway Test Sites*. Georgia Pavement and Traffic Research Center, Southern Polytechnic State University, Marietta, GA

17. Kim and Pahno. (2019). *Prediction of Resilient Modulus from the Laboratory Testing of Sandy Soils*. University of Georgia, Athens, GA.

18. Park, Bobet, and Nantung (2018). Correlation between Resilient Modulus Mr of Soil, Light Weight Deflectometer (LWD), and Falling Weight Deflectometer (FWD). Joint Transportation Research Program. West Lafayette, IN.

19. Pavement Interactive. AASHTO Road Test. https://pavementinteractive.org/reference-desk/design/structural-design/aasho-road-test/ Accessed 12/01/2021.

20. The Asphalt Institute (1982), "Research and Development of the Asphalt Institute's Thickness Design Manual, Ninth Edition," Research Report No. 82-2.

21. Tihey and Kim S.H. (2020). Estimation of Resilient Modulus for Fine-Grained Soils Using Ground Penetrating Radar. Athens, GA.

22. Topp, G.C., Davis, J.L., & Annan, A.P. (1980). Electromagnetic determination of soil water content: Measurements in coaxial transmission lines. *Water Resources Research*, Vol. 16, No. 3, Pages 574-582.

Appendix

GEORGIA SR 10 ROADWAY DATA

EASTBOUND

FWD Field Data - RAW

Station ID.	Drop ID.	TEMP (F.)	STATION (ft.)	LATITUDE	LONGITUDE	FORCE (lbs)	Displacement Sensors (mils) d1 (0)	d2 (8")	d3 (12")	d4 (18")	d5 (24")	d6 (36")	d7 (60")	d8 (96")	d9 (120")
1	1	88.30	0.00	33.83020231110	-83.86587621160	6503	6.07000	4.91000	4.22000	3.64000	3.14000	2.40000	1.70000	1.26000	0.98000
1	2	88.30	0.00	33.83020231110	-83.86587621160	6503	6.05000	4.88000	4.22000	3.64000	3.13000	2.39000	1.72000	1.30000	1.05000
1	3	88.30	0.00	33.83020231110	-83.86587621160	9196	8.66000	7.13000	6.16000	5.35000	4.62000	3.53000	2.55000	1.91000	1.50000
1	4	88.30	0.00	33.83020231110	-83.86587621160	9167	8.65000	7.13000	6.18000	5.36000	4.63000	3.50000	2.57000	1.93000	1.52000
1	5	88.20	0.00	33.83020231110	-83.86587621160	11947	11.39000	9.42000	8.17000	7.15000	6.16000	4.67000	3.43000	2.56000	2.01000
1	6	88.20	0.00	33.83020231110	-83.86587621160	11900	11.36000	9.44000	8.14000	7.14000	6.18000	4.71000	3.46000	2.56000	2.00000
2	7	88.80	101.10	33.83017754100	-83.86555742700	6434	3.84000	3.13000	2.78000	2.39000	2.03000	1.49000	1.11000	0.85000	0.68000
2	8	88.80	101.10	33.83017754100	-83.86555742700	6439	3.84000	3.16000	2.80000	2.43000	2.06000	1.53000	1.14000	0.87000	0.71000
2	9	88.70	101.10	33.83017754100	-83.86555742700	9148	5.41000	4.45000	3.92000	3.37000	2.88000	2.15000	1.56000	1.24000	1.02000
2	10	88.70	101.10	33.83017754100	-83.86555742700	9132	5.37000	4.45000	3.92000	3.39000	2.89000	2.12000	1.57000	1.25000	1.04000
2	11	88.70	101.10	33.83017754100	-83.86555742700	11947	6.90000	5.73000	5.07000	4.43000	3.81000	2.83000	2.20000	1.69000	1.36000
2	12	88.60	101.10	33.83017754100	-83.86555742700	11916	6.92000	5.73000	5.07000	4.42000	3.80000	2.82000	2.17000	1.70000	1.38000
3	13	91.90	197.30	33.83015406900	-83.86524104100	6514	8.80000	6.87000	6.09000	5.31000	4.57000	3.40000	2.51000	1.81000	1.34000
3	14	91.90	197.30	33.83015406900	-83.86524104100	6506	8.72000	6.83000	6.08000	5.29000	4.56000	3.40000	2.51000	1.82000	1.35000
3	15	91.80	197.30	33.83015406900	-83.86524104100	9183	12.53000	9.94000	8.84000	7.75000	6.67000	5.00000	3.65000	2.63000	1.93000
3	16	91.80	197.30	33.83015406900	-83.86524104100	9156	12.54000	9.98000	8.90000	7.81000	6.73000	5.08000	3.72000	2.69000	1.96000
3	17	91.70	197.30	33.83015406900	-83.86524104100	11896	16.36000	13.21000	11.75000	10.41000	8.98000	6.86000	5.01000	3.61000	2.63000
3	18	91.70	197.30	33.83015406900	-83.86524104100	11852	16.38000	13.24000	11.80000	10.49000	9.05000	6.97000	5.09000	3.68000	2.68000
4	19	91.10	300.50	33.83012720900	-83.86489940200	6387	6.24000	5.05000	4.47000	3.93000	3.40000	2.59000	1.94000	1.43000	1.15000
4	20	91.10	300.50	33.83012720900	-83.86489940200	6395	6.28000	5.10000	4.54000	4.00000	3.46000	2.63000	2.02000	1.46000	1.19000
4	21	91.10	300.50	33.83012720900	-83.86489940200	9064	9.05000	7.39000	6.60000	5.81000	5.07000	3.91000	2.92000	2.22000	1.75000
4	22	91.00	300.50	33.83012720900	-83.86489940200	9056	9.07000	7.41000	6.61000	5.84000	5.10000	3.90000	2.97000	2.25000	1.79000
4	23	91.00	300.50	33.83012720900	-83.86489940200	11828	11.88000	9.77000	8.74000	7.74000	6.78000	5.27000	3.96000	3.01000	2.38000
4	24	91.00	300.50	33.83012720900	-83.86489940200	11788	11.86000	9.77000	8.73000	7.74000	6.79000	5.28000	3.98000	3.03000	2.39000
5	25	92.00	411.50	33.83009790200	-83.86453485600	6450	5.28000	3.98000	3.28000	2.62000	2.18000	1.39000	0.88000	0.57000	0.45000
5	26	91.90	411.50	33.83009790200	-83.86453485600	6442	5.25000	3.98000	3.28000	2.61000	2.19000	1.37000	0.89000	0.57000	0.46000
5	27	91.90	411.50	33.83009790200	-83.86453485600	9156	7.39000	5.61000	4.66000	3.71000	3.11000	1.96000	1.30000	0.82000	0.66000
5	28	91.80	411.50	33.83009790200	-83.86453485600	9135	7.38000	5.59000	4.65000	3.69000	3.13000	1.97000	1.32000	0.83000	0.68000
5	29	91.80	411.50	33.83009790200	-83.86453485600	11944	9.52000	7.23000	6.04000	4.84000	4.07000	2.59000	1.71000	1.13000	0.91000
5	30	91.70	411.50	33.83009790200	-83.86453485600	11900	9.50000	7.23000	6.04000	4.84000	4.09000	2.64000	1.74000	1.17000	0.94000
6	31	91.30	506.50	33.83007275300	-83.86422178400	6392	4.71000	3.43000	2.74000	2.10000	1.51000	0.93000	0.56000	0.42000	0.36000
6	32	91.30	506.50	33.83007275300	-83.86422178400	6392	4.72000	3.43000	2.74000	2.11000	1.52000	0.93000	0.56000	0.43000	0.37000
6	33	91.20	506.50	33.83007275300	-83.86422178400	9080	6.61000	4.83000	3.90000	3.02000	2.19000	1.37000	0.81000	0.62000	0.53000
6	34	91.20	506.50	33.83007275300	-83.86422178400	9064	6.56000	4.80000	3.87000	2.99000	2.18000	1.37000	0.80000	0.61000	0.51000
6	35	91.10	506.50	33.83007275300	-83.86422178400	11876	8.48000	6.24000	5.04000	3.93000	2.87000	1.81000	1.07000	0.81000	0.68000
6	36	91.10	506.50	33.83007275300	-83.86422178400	11844	8.43000	6.20000	5.02000	3.91000	2.86000	1.80000	1.06000	0.81000	0.67000
7	37	91.30	602.60	33.83004795500	-83.86390563900	6392	5.69000	4.34000	3.76000	2.98000	2.43000	1.71000	1.25000	1.01000	0.87000
7	38	91.30	602.60	33.83004795500	-83.86390563900	6387	5.66000	4.37000	3.76000	3.02000	2.46000	1.66000	1.30000	1.01000	0.91000
7	39	91.20	602.60	33.83004795500	-83.86390563900	9080	8.00000	6.16000	5.34000	4.29000	3.50000	2.40000	1.83000	1.46000	1.28000
7	40	91.20	602.60	33.83004795500	-83.86390563900	9064	7.99000	6.15000	5.34000	4.26000	3.48000	2.44000	1.83000	1.48000	1.27000
7	41	91.20	602.60	33.83004795500	-83.86390563900	11860	10.31000	8.00000	6.96000	5.62000	4.58000	3.22000	2.41000	1.94000	1.69000
7	42	91.20	602.60	33.83004795500	-83.86390563900	11820	10.27000	7.99000	6.95000	5.61000	4.57000	3.21000	2.40000	1.93000	1.67000

Figure 31: Raw FWD Dataset for SR10 Eastbound

9 KIP NORMALIZATION															
Station ID.	Drop ID.	PAVE TEMP (F.)	STATION (ft.)	LATITUDE	LONGITUDE	FORCE (LBS)	Displacement Sensors (mils)								
							d1 (0)	d2 (8")	d3 (12")	d4 (18")	d5 (24")	d6 (36")	d7 (60")	d8 (96")	d9 (120")
1	3	88.30	0.00	33.830202311100	-83.865876211605	9000	8.475424	6.978034	6.028708	5.235972	4.521531	3.454763	2.495650	1.869291	1.468030
1	4	88.30	0.00	33.830202311100	-83.865876211605	9000	8.492418	7.000109	6.067416	5.262354	4.545653	3.436239	2.523181	1.894840	1.492309
2	9	88.70	101.10	33.830177541000	-83.865557427001	9000	5.322475	4.378006	3.856581	3.315479	2.833406	2.115217	1.534762	1.219939	1.003498
2	10	88.70	101.10	33.830177541000	-83.865557427001	9000	5.292378	4.385677	3.863338	3.340999	2.848226	2.089356	1.547306	1.231932	1.024967
3	15	91.80	197.30	33.830154069000	-83.865241041000	9000	12.280300	9.741914	8.663835	7.595557	6.537079	4.900359	3.577262	2.577589	1.891539
3	16	91.80	197.30	33.830154069000	-83.865241041000	9000	12.326343	9.809960	8.748361	7.676933	6.615334	4.993447	3.656619	2.644168	1.926606
4	21	91.10	300.50	33.830127209000	-83.864899402000	9000	8.986099	7.337820	6.553398	5.768976	5.034201	3.882392	2.899382	2.204325	1.737643
4	22	91.00	300.50	33.830127209000	-83.864899402000	9000	9.013913	7.364178	6.569126	5.803887	5.068463	3.875883	2.951634	2.236087	1.778931
5	27	91.90	411.50	33.830097902000	-83.864534856000	9000	7.264089	5.514417	4.580603	3.646789	3.057012	1.926606	1.277851	0.806029	0.648755
5	28	91.80	411.50	33.830097902000	-83.864534856000	9000	7.270936	5.507389	4.581281	3.635468	3.083744	1.940887	1.300493	0.817734	0.669951
6	33	91.20	506.50	33.830072753000	-83.864221784000	9000	6.551762	4.787445	3.865639	2.993392	2.170705	1.357930	0.802863	0.614537	0.525330
6	34	91.20	506.50	33.830072753000	-83.864221784000	9000	6.513680	4.766108	3.842674	2.968888	2.164607	1.360327	0.794351	0.605693	0.506399
7	39	91.20	602.60	33.830047955000	-83.863905639000	9000	7.929515	6.105727	5.292952	4.252203	3.469163	2.378855	1.813877	1.447137	1.268722
7	40	91.20	602.60	33.830047955000	-83.863905639000	9000	7.933583	6.106576	5.302295	4.229921	3.455428	2.422771	1.817079	1.469550	1.261033
8	45	91.00	720.30	33.830020255000	-83.863516442000	9000	12.090000	10.930000	9.840000	8.720000	7.690000	6.010000	4.720000	3.570000	2.910000
8	46	90.90	720.30	33.830020255000	-83.863516442000	9000	12.100756	10.899689	9.838745	8.697731	7.686833	6.065391	4.724199	3.633230	2.962633
9	51	91.30	802.00	33.829999143000	-83.863247140000	9000	10.528075	9.445187	8.743316	7.911096	7.108957	5.705214	4.471925	3.529412	2.827540
9	52	91.30	802.00	33.829999143000	-83.863247140000	9000	10.551032	9.446737	8.744005	7.920803	7.137758	5.752370	4.517568	3.593976	2.901283
10	57	90.90	901.90	33.829972626000	-83.862916851999	9000	9.073869	7.945874	7.237134	6.458518	5.799689	4.671695	3.643523	2.874889	2.325865
10	58	90.80	901.90	33.829972626000	-83.862916851999	9000	9.060000	7.930000	7.240000	6.480000	5.800000	4.700000	3.660000	2.900000	2.350000
11	63	90.00	1001.00	33.829945852000	-83.862590960999	9000	7.722542	6.197963	5.301152	4.414305	3.726749	2.770151	2.172276	1.693977	1.414969
11	64	90.00	1001.00	33.829945852000	-83.862590960999	9000	7.678908	6.161101	5.292356	4.403639	3.714634	2.736048	2.186841	1.687562	1.387995
12	69	89.80	1103.30	33.829920725000	-83.862255083000	9000	12.536569	10.142952	8.567154	6.811835	5.415558	3.530585	2.263963	1.565825	1.236702
12	70	89.70	1103.30	33.829920725000	-83.862255083000	9000	12.517746	10.151952	8.564774	6.837844	5.420364	3.553682	2.275954	1.567214	1.257764
13	75	91.40	1199.90	33.829897034000	-83.861935293001	9000	13.319722	10.826619	9.187728	7.270721	5.850348	3.724754	2.373910	1.579296	1.102527
13	76	91.30	1199.90	33.829897034000	-83.861935293001	9000	13.345136	10.895208	9.251964	7.339825	5.925639	3.784442	2.420051	1.613367	1.125373
14	81	89.80	1301.90	33.829869982733	-83.861597136469	9000	12.129353	9.890547	8.427861	6.815920	5.263682	3.373134	2.099502	1.402985	1.124378
14	82	89.80	1301.90	33.829869982733	-83.861597136469	9000	12.182403	9.945634	8.487740	6.870077	5.312327	3.425053	2.166870	1.467880	1.188284
15	87	91.60	1399.30	33.829844456000	-83.861278529999	9000	11.133401	9.317954	8.264794	7.221665	6.238716	4.844534	3.610832	2.828485	2.306921
15	88	91.60	1399.30	33.829844456000	-83.861278529999	9000	11.143240	9.344647	8.289606	7.244613	6.249860	4.853187	3.637378	2.863682	2.341186
16	93	92.60	1495.50	33.829818135000	-83.860963459000	9000	12.255791	10.946626	10.251763	9.274925	8.449144	6.727089	5.226586	4.048338	3.222558
16	94	92.60	1495.50	33.829818135000	-83.860963459000	9000	12.302085	10.990133	10.293788	9.335053	8.477237	6.791882	5.267997	4.107423	3.289975
17	99	93.50	1574.70	33.829798883000	-83.860702569000	9000	7.173262	6.135684	5.537080	4.748919	4.050549	2.963086	2.125042	1.606252	1.306950
17	100	93.50	1574.70	33.829798883000	-83.860702569000	9000	7.190000	6.150000	5.540000	4.760000	4.050000	2.980000	2.130000	1.600000	1.310000
18	105	94.20	1608.60	33.829791015000	-83.860589887000	9000	8.744052	6.991258	5.875844	4.262477	3.555383	2.270665	1.513777	1.105455	0.906274
18	106	94.20	1608.60	33.829791015000	-83.860589887000	9000	8.706781	6.981383	5.864362	4.258644	3.550532	2.253989	1.515957	1.097074	0.897606
19	111	92.60	1698.50	33.829766412000	-83.860292686000	9000	11.851893	9.700659	8.635095	7.418742	6.262705	4.332626	2.875014	1.930079	1.367140
19	112	92.60	1698.50	33.829766412000	-83.860292686000	9000	11.883182	9.718026	8.650554	7.442095	6.283988	4.350453	2.910373	1.953676	1.379658
20	117	95.20	1796.80	33.829738898000	-83.859970856999	9000	9.370000	7.970000	7.060000	5.880000	4.850000	3.190000	2.010000	1.290000	0.960000

Figure 32: SR 10 Eastbound 9-Kip Normalized Load

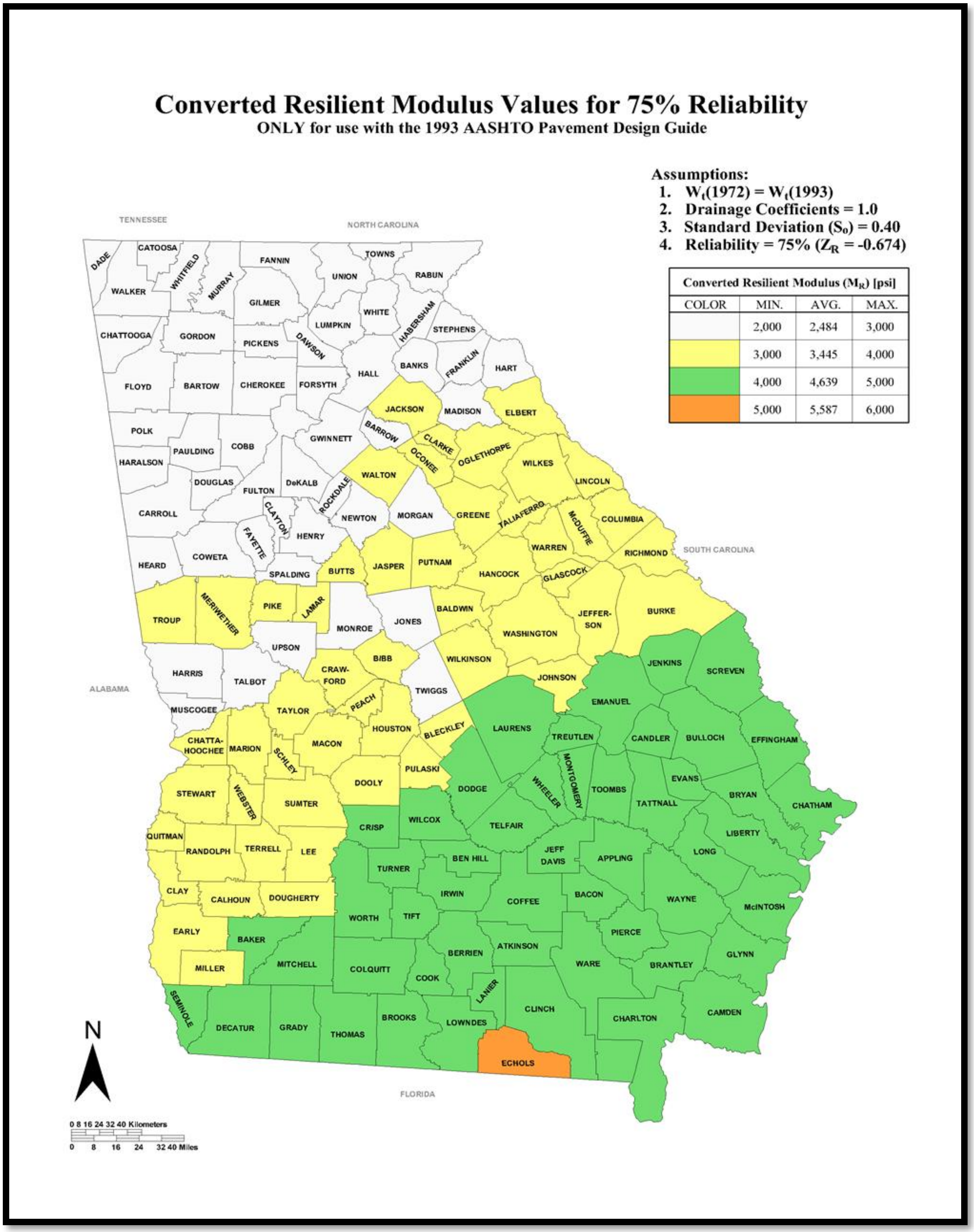

Figure 33: 75% Reliability Mr Map

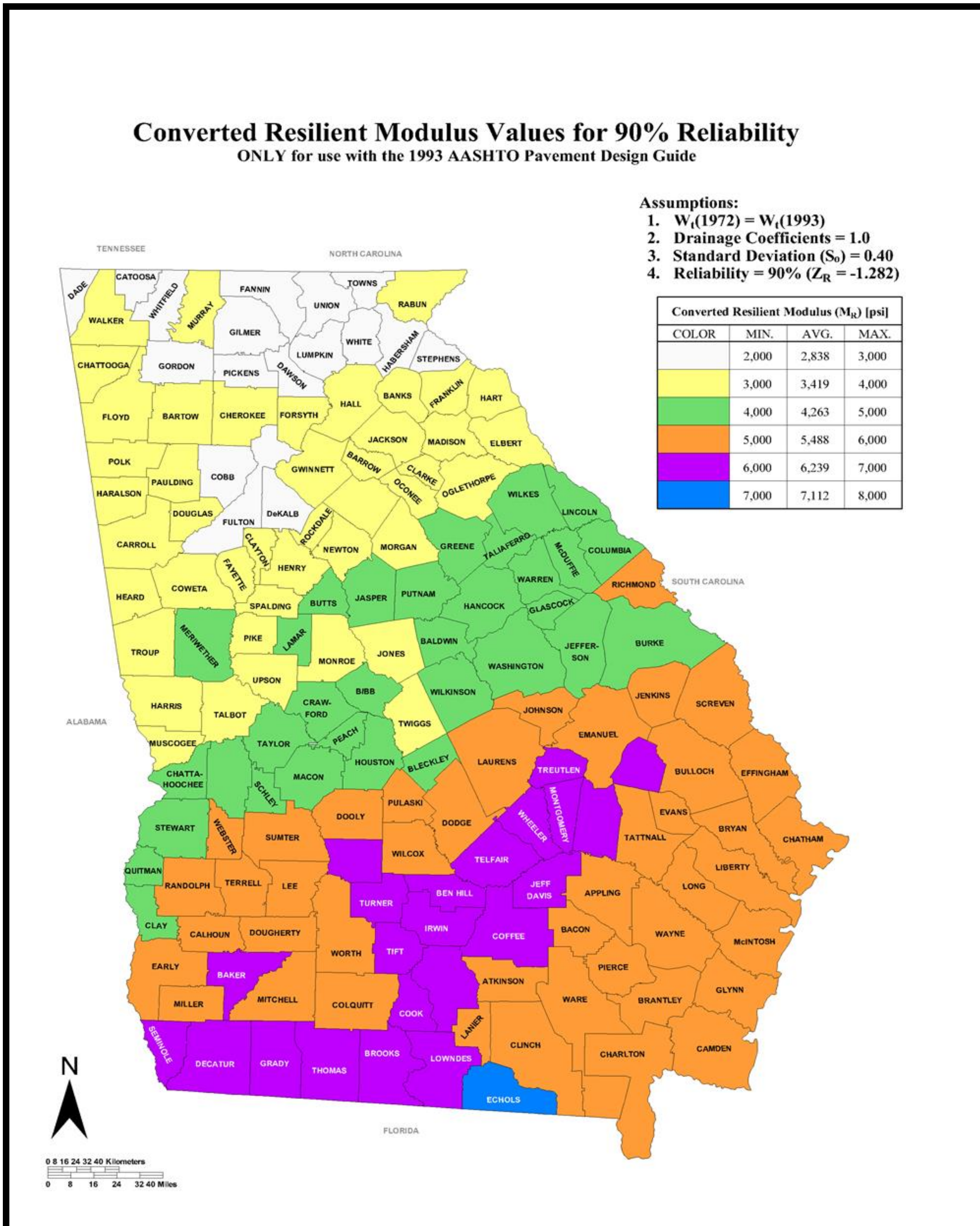

Figure 34: 90% Reliability Mr Map